Mardi et al., *BioImpacts.* 2026;16:33180
doi:10.34172/bi.33180
https://bi.tbzmed.ac.ir/

Targeted delivery of doxorubicin using RSV F-protein modified breast cancer-derived exosomes in breast cancer-bearing mice

Narges Mardi[1,2], Amir Zarebkohan[3], Cigir Biray-Avci[4], Reza Rahbarghazi[5], Mehdi Talebi[5,6], Hamid Lotfimehr[5], Sharareh Khavandkari[7], Zahra Abbasi-Malati[5], Nastaran Sedghi-Samarkhazan[8], Elham Shahriyari[4], Asghar Khalilnezhad[4], Morteza Milani[1*], Mohammad Nouri[1*]

[1]Department of Medical Biotechnology, Faculty of Advanced Medical Sciences, Tabriz University of Medical Sciences, Tabriz, Iran
[2]Biotechnology Research Center, Tabriz University of Medical Sciences, Tabriz, Iran
[3]Department of Medical Nanotechnology, Faculty of Advanced Medical Sciences, Tabriz University of Medical Sciences, Tabriz, Iran
[4]Department of Medical Biology, Faculty of Medicine, Ege University, Izmir, Turkey
[5]Department of Applied Cell Sciences, Faculty of Advanced Medical Sciences, Tabriz University of Medical Sciences, Tabriz, Iran
[6]Hematology and Oncology Research Center, Tabriz University of Medical Sciences, Tabriz, Iran
[7]Department of Animal Biology, Faculty of Natural Sciences, University of Tabriz, Tabriz, Iran
[8]Department of Biology, Faculty of Science, University of Guilan, Rasht, Iran

Article Info

Article Type:
Original Article

Article History:
Received: 22 Nov. 2025
Accepted: 25 Jan. 2026
ePublished: 15 Jun. 2026

Keywords:
Modified exosomes
Fusion protein of RSV
Targeted delivery
Breast cancer

Abstract

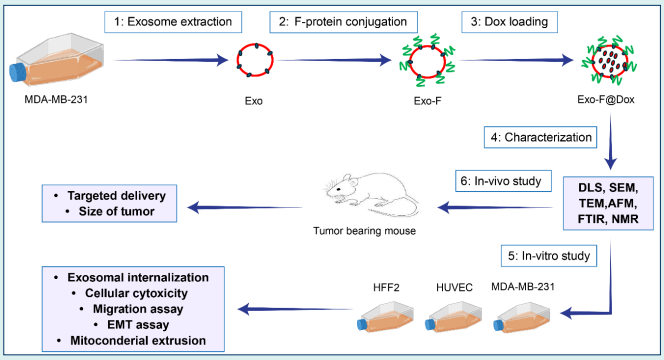

Introduction: Triple-negative breast cancer demonstrated high metastasis and mortality rates in female populations. Emerging data on effective targeting and specific internalization of chemotherapeutic agents, using modified exosomes, decreased the therapeutic dosage of anti-cancer drugs in cancer cells.

Methods: Herein, we developed modified exosomes by surface decoration using the Fusion protein of Respiratory Syncytial Virus (F-protein of RSV) through Click-chemistry techniques, and Dox-loaded via sonication strategy. Then, the viability and metastatic behaviors of MDA-MB-231 cells were monitored in the presence of different groups, including Dox, Exosomes (Exo), Exosomes loaded with Dox (Exo@Dox), and F-protein coupled Exosome groups (Exo-F) and (Exo-F@Dox).

Results: In vitro and in vivo results verified that the F-protein coupled exosome, as a modified natural nanoplatform, possessed a biocompatible nature in blood circulation and crossing of blood barriers. After exposure to tumoral temperature (40 °C) and lysosomal PH (5.5) demonstrate amplified Dox release (around 60% at 8 h). Also, in vitro uptake results confirmed a significant increase in Exo-F internalization compared to the Exo group in MDA-MB-231 cells ($P<0.0001$). Correspondingly, the IC50 value of Exo-F@Dox versus free Dox showed a significant reduction (24-fold more potent) ($P<0.0001$). Interestingly, Dox-free modified Exo (Exo-F) showed appreciable cytotoxicity (IC50 of about 0.1 µg /mL for exosomal protein concentration) ($P<0.0001$). Also, migration assay results confirmed a considerable decrease in the migrated population of MDA-MB-231 cells (10%) compared to the control group, following exposure to modified exosomes. Interestingly, an in vivo study in tumor-bearing Balb/c mice demonstrated a significantly decreased tumor size in the Exo-F groups compared to other formulations.

Conclusion: In summary, F-protein modified exosomes exhibited superior anticancer efficacy by improving tumor-specific targeting, ensuring precise delivery of chemotherapeutic agents, facilitating efficient drug release, and allowing for lower therapeutic dosages.

*Corresponding authors: Mohammad Nouri, Email: nourimd@yahoo.com; Morteza Milani, Email: mohammadmilano@gmail.com

Research Highlights

What is the current knowledge?

- The role of the viral Fusion protein has been proven in the development of viral attachment to the recipient cells.

What is new here?

- Fusion protein-coupled Exosomes induce higher uptake and cytotoxicity and inhibit migration of the tumoral cells, more than free Dox.
- Modified Exosomes led to changes in the EMT pathway.
- Modified Exosomes induce targeted delivery of particles to tumoral cells in vitro and in vivo.

Introduction

Respiratory syncytial virus (RSV), which belongs to the human Pneumoviridae family, is a pathogenic agent responsible for acute lower respiratory tract infections in infants, the elderly, and immunocompromised patients.[1,2] RSV infection activates the innate immune response, causing the release of chemokines and cytokines that lead entrapment of neutrophils in the respiratory tract and finally induce the neutrophil extracellular trap process (known as NETosis).[3,4] It has been reported that both RSV particles and the RSV fusion protein (F-protein) promote NETosis by attracting neutrophils.[3,5] Based on evidence, the interaction of RSV F-protein with TLR-4 on the surface of target cells stimulates the release of neutrophil extracellular traps (NETs).[5] NETs, which consist of protein-coated nucleic acids released from neutrophils have been shown to trap cancer cells and stimulate cancer growth.[6] The RSV fusion (F) protein, a viral transmembrane binding protein, accelerates fusion of the RSV particle with host cells. In addition, F-protein–mediated activation of the RhoA signaling pathway causes fusion of infected cells with adjacent cells and formation of multinucleated syncytia.[7,8]

Schlender et al. demonstrated that RSV F-protein inhibits mitogen-promoted proliferation of T-cells.[9] Furthermore, Eckardt-Michael et al. showed that expression of RSV F-protein induces programmed cell death through activation of p53 and promotion of caspase-dependent apoptosis, leading to loss of epithelial integrity and separation of apoptotic cells from the polarized epithelial cells.[7] On the other hand, the strong potential of RSV F-protein to physically interact with several cellular receptors -including MD-2, TLR-4, insulin-like growth factor 1 receptor (IGF1R), Nucleolin- and to activate proinflammatory cytokines signaling upon recognition by cellular receptors,[10,11] supports the concept that conjugation of RSV F-protein onto the surface of a carrier may provide a ligand for efficient internalization into specialized tissues, and promote the therapeutic effects of the medicine.. exosomes were first described as carriers of cellular waste in the early 1980s by Penn and Johnston.[12] Over the last two decades, research on exosomes -small extracellular vesicles with diameters ranging from 30 to 200 nm which act as biological tools in the dissemination of paracrine activity from cell to cell- has attracted increasing attention.[13] Meanwhile, the ability of exosomes to transport a wide variety of biomolecules, such as growth factors, lipids, proteins, and nucleic acids (e.g. DNA, mitochondrial DNA, miRNAs, and circRNA), underscores their potential as therapeutic carriers.[14] These properties promoted extensive investigations into biomedical applications of exosomes, including tissue regeneration,[15] drug delivery, gene therapy,[16] cancer treatment and diagnosis,[17] and vaccine development.[18] Despite our knowledge of the contents and physicochemical properties of exosomes, the use of exosomes as a suitable therapeutic or diagnostic platform still faces significant challenges and limitations.[19] At the same time, the use of exosomes as natural carriers lacks some properties required for the development of effective therapeutic targeting. In particular, in cancer therapy, specific targeting of cancer cells by therapeutic exosomes is considered essential. Furthermore, in some cases, it is necessary to load exogenous molecules -such as a protein, RNAs, or small-molecule drugs- into exosomes to achieve a therapeutic effect. Fortunately, biotechnological advances have led to the emergence of a new therapeutic field known as “exosome engineering”.[12] Nevertheless, the application of natural exosomes as therapeutic agents in cancer treatment remains challenging. Generally, natural exosomes exhibit limited cell- or tissue-specific targeting capability.[12] Therefore, to enable the therapeutic use of exosomes as efficient delivery systems, the design of targeted exosomes is essential. Furthermore, to broaden the clinical applicability of exosomes, there is a need to load specific therapeutic molecules into exosomes through the development of effective loading techniques. In this regard, exosome engineering techniques, such as exploiting the functional ligand-receptor system, increasing the density of a specific molecule in exosomes, facilitate the development of engineered exosomes with enhanced targeting specificity or with defined therapeutic abilities. These strategies have the potential to overcome the limitations of natural exosomes in cancer therapy. Chemotherapeutic drugs, as the cornerstone of cancer treatment, are often associated with significant side effects, including hematologic toxicity,[20] gastrointestinal toxicity,[21] alopecia,[22] cardiotoxicity,[23] neuro-, renal-, and hepatic-toxicity.[24,25] These toxicities emanate from the off-target nature of conventional chemotherapy.[26] Doxorubicin (Dox), a widely used chemotherapeutic agent and DNA topoisomerase II inhibitor, leads to cellular death by arresting DNA repair and by inducing oxidative stress within cellular membranes.[27,28] Drug resistance to Dox in Triple-negative breast cancer (TNBC) is mostly attributed with multiple mechanisms, including the over-expression of drug efflux pumps such as P-glycoprotein, and shifting the drug metabolism pathways.[26]

Breast cancer is one of the most commonly diagnosed cancers among females worldwide. Among the various breast cancer subtypes, TNBC is characterized by

its invasive nature, poor prognosis, and frequent development of drug resistance. TNBC is known by negative expression of three receptors: progesterone receptor (PR) and estrogen receptor (ER), and the human epidermal growth factor receptor 2 (HER2).[27,29,30] The studies have indicated that MDA-MB-231 cells, a model for aggressive breast cancer, show overexpression of epidermal growth factor receptor (EGFR). Moreover, evidence suggests that positive EGFR expression is associated with upregulation of Nucleolin, IGF1, CD14, and a subsets of Toll-like receptor 4 (TLR4)-responsive genes. According to a wide range of studies TNBC tumors shown high expression repertoire of TLR4, Nucleolin, and IGF1, that unfortunately related to poor prognosis of breast cancer patients.[31-35] On the other hand, F-protein of RSV has been candidate for serving as an efficient ligand for these receptors. Interestingly, RSV F-protein could be served as a ligand previously.[36-38] Also, the MDA-MB-231 cell line has been demonstrated to show cancer stem cell (CSC)-like properties.[39] Accordingly, throughout this manuscript, these cells are considered representative of CSC-like tumor cells.

In the present study, RSV F-protein was covalently conjugated onto the surface of MDA-MB-231-derived exosomes using an EDC/NHS click chemistry strategy. We postulated that conjugation of RSV F-protein on the surface of exosomes as a targeting ligand, induces higher efficacy in the internalization and enables targeted delivery of Dox into MDA-MB231 cells. Accordingly, we hypothesized that conjugation of RSV F-protein onto the exosome surface would promote specialized internalization, increase cancer cell death, and inhibit the migration and invasion of cancer cells.

Materials and Methods

Cells and culture environment

MDAMB-231 cell line, as a cancer stem cell line, HUVEC (human umbilical vein endothelial cell line), HFF2 (human fibroblast cell line) as normal non-cancerous cell lines, and 4T1 (mouse breast cancer cell line) were provided from the Pasteur Institute Culture Collection (Tehran, Iran), and were then cultured in Gibco's (USA) Roswell Park Memorial Institute (RPMI) 1640 medium supplemented with 10% (v/v) FBS and 1% penicillin/streptomycin at 37 ˚C in a humidified atmosphere containing 5% CO_2 up to passage 6.

Animal model

All animals were treated in accordance with the Ethics Committee at Tabriz University of Medical Sciences, Iran, under ethical approval number IR.TBZMED.VCR.REC.1400.158. Female BALB/c mice, six weeks old and weighing approximately 20 g, were obtained from the Iranian company Pishro Mehravaran Azma Pars. The mice were maintained under standard conditions and allowed to acclimate to their environment before establishing of the tumor model. To generate the model, 1.5×10^6 4T1 cells were injected intraperitoneally into the right flank of each mouse. After the tumor reached a size of 50 mm^3 within 21 days, different exosome formulations were administrated at a dose of 30 µg exosomal protein per mouse every three days for a total of three doses, with a final injection volume of 100 µL.

Isolation of exosomes

The MDA-MB-231 cell culture at approximately 70%–80% confluence was incubated in Dulbecco's Modified Eagle Medium (DMEM) supplemented with 10% exosome-free FBS for exosome secretion. The culture supernatant was then collected and subjected to clarification by serial centrifugation (10 min in 300 x g to remove cell debris, 20 min in 1500 x g to remove cell fragments, and 30 min in 13000 x g at 4 °C to remove cellular organelles, apoptotic bodies and large microvesicles). The resulting supernatant was filtered through a 0.22 µm filter and ultracentrifuged at 120,000 x g, at 4 °C for 16 min to harvest the exosomal pellet. Subsequently, the supernatant was discarded, and the exosomes were resuspended in 500 µL of cold PBS (pH:7,4) and stored at -70 °C for further investigations.

Western blot analysis

Exosomal membrane markers, including CD9, CD63, and CD81, were analyzed by Western blot analysis. In this regard, the exosome suspension was lysed using radioimmunoprecipitation Assay (RIPA) lysis buffer and then centrifuged at 13,000×g for 10 min at 4 °C. The lysate samples were used for separation protein separation by 10% sodium dodecyl sulfate polyacrylamide gel electrophoresis (SDS-PAGE), and the separated proteins were subsequently transferred onto 0.2 µm PVDF membranes. The membranes were blocked with 1% bovine serum albumin (BSA; Sigma-Aldrich) for 1 h at room temperature. After three washes with PBST, the PVDF membranes were incubated overnight at 4 ˚C with primary antibodies, including anti-human CD63 (Cat. No. sc-5275; Santa Cruz Biotechnology), anti-human CD81 (Cat. No. sc-166029; Santa Cruz Biotechnology), and anti-human CD9 (Cat. No. sc-13118; Santa Cruz Biotechnology). Following washing with PBST, the membranes were incubated with horseradish peroxidase (HRP) -conjugated secondary antibodies (Cat. No. sc-516102; Santa Cruz Biotechnology) for 1 h at room temperature. Subsequently, the membranes were washed and incubated with enhanced chemiluminescence solution (Bio-Rad). Finally, immunoreactive protein bands were visualized using X-ray film.

Exosomal protein concentration measurement

To estimate the EV content obtained from the isolation process, the protein concentration of purified EV suspensions was quantified using a bicinchoninic acid (BCA) protein assay kit (Thermo Fisher Scientific, Cat. No. 23227) according to the manufacturer's instructions. Briefly, quantification was performed by preparing a serial dilution to generate a standard curve. Subsequently, exosome concentration was determined based on the standard curve.

Surface modification of exosomes

The covalent conjugation of F-protein (RSV fusion protein) onto the surface of exosomes was performed using standard carbodiimide chemistry (click chemistry). In this procedure, a 1:1:1 molar ratio of EDC: NHS: F-Protein and a 20% (w/w) protein-to-exosome ratio were used. For this purpose, the exosome solution (250 µL, 1.5 mg/mL) was added to EDC (82 µL, 1 mg/mL) and incubated for 30 min to activate carboxyl groups. Subsequently, NHS (110 µL,1 mg/mL) was added, and the mixture was shaken at 37 ˚C for 1 h generate activated amino-reactive intermediates on the exosomes surface. Then, 100µL of F-protein (0.5 mg/mL) was added to the reaction mixture. Finally, 500 µL of PBS buffer (100 mM, pH 7.4) was added. The solution was subjected to dialysis (MWCO 14 kDa, Sigma Aldrich) and shaken at 250 rpm overnight to remove unbonded Proteins. The F-protein-conjugated exosomes were then collected from the dialysis bag.

Calculation of modification efficiency

For the evaluation of the efficiency of the EDC-NHS system and quantification of the F-protein bound to the surface of exosomes, the BCA Protein Quantitation Kit was used. Specifically, quantification of surface-bound F-protein was performed indirectly by measuring the amount of unbound F-protein and comparing it with a standard curve generated using serial protein dilutions. The efficiency of the EDC-NHS system and the bounding efficiency were calculated using the following formula:

$$\text{Binding Capicity}(\%) = \frac{\text{Total amount of peptide} - \text{Unbounded peptide}}{\text{Weight of nanoparticle}} \times 100 \quad \text{Eq. 1}$$

$$\text{Binding Efficiency}(\%) = \frac{\text{Total amount of peptide} - \text{Unbounded peptide}}{\text{Total protein}} \times 100 \quad \text{Eq. 2}$$

Characterization of exosomal modifications

All exosome extraction, modification, and loading steps were confirmed by dynamic light scattering (DLS) using a Malvern Particle Sizer (Zetasizer Nano ZS90, United Kingdom) to determine the average hydrodynamic diameter and zeta potential of different exosome formulations (Exo, Exo-F, Exo@Dox, Exo-F@Dox). The morphology and surface alterations of the exosome formulations were assessed using scanning electron microscopy (SEM; MIRA3 FEG-SEM, Tescan, Czech Republic) and transmission electron microscopy (TEM; LEO 906, Zeiss, Germany), respectively. In addition, analysis of the three-dimensional surface topography of modified exosomes at the atomic level was performed using atomic force microscopy (AFM; Bruker - NanoWizard II, Germany). Each exosomal modification step was further confirmed by proton nuclear magnetic resonance (^{1}H-NMR) spectroscopy (Bruker SpectroSpin Avance spectrometer, Germany), and Fourier transform infrared (FT-IR) Spectroscopy (Bruker-Tensor 27, Germany).

Drug loading study

In this regard, IC_{50} concentration of Dox (Doxorubicin Hydrochloride; EBEWE Pharma AUSTRIA, Lot. No. LP5345; was purchased from Tabriz university of medical sciences pharmacy (Iran).) was mixed with exosome groups (Exo, Exo-F) at 30 µg /mL exosomal protein and sonicated using a probe sonicator with a 25" tip at 20% amplitude for 6 cycles of 30 s, with a 2 min cooling period between each cycle in an ice bath. The sonicated mixture (Exo-Dox solution) was then incubated for 60 min at 37 ˚C to allow recover of the exosome membrane. Subsequently, to separate unloaded free Dox from Dox-loaded exosomes, the mixture was sedimented by ultracentrifugation at 90,0000×g for 60 min at 4 °C. Finally, the exosomal pellets were collected and resuspended in PBS. Thereafter, loading of Dox into the exosomes was confirmed by DLS, SEM, and TEM analyses through an increase in particle size and a shift in zeta potential. In addition, the amount of drug loading and release was evaluated at a wavelength of 490 nm using a UV-vis spectrophotometer. The quantity of drug loading was measured using a UV-vis spectrophotometer (Scinco 4100 spectrophotometer, Shimadzu, Japan) at a wavelength of 490 nm. The drug encapsulation efficiency and loading capacity of the exosomes were calculated using the following formula:

$$\text{ELoading Capicity}(\%) = \frac{\text{Total DOX} - \text{Supernatant DOX}}{\text{Total weight of exosomes}} \times 100 \quad \text{Eq. 3}$$

$$\text{Encapsulation Efficiency}(\%) = \frac{\text{Total DOX} - \text{Supernatant DOX}}{\text{Total DOX}} \times 100 \quad \text{Eq. 4}$$

Surface interaction of exosomes with the cells

For examination of surface physical interactions of exosomes, 4×10^5 MDA-MB-231 cells were cultured under standard conditions on the surface of Au SPR chip and allowed to form a monolayer on the Au chip. After washing, the chips were placed in an SPR instrument (MP-SPR Navi 210A, BioNavis Ltd., Tampere, Finland). exosomes (Exo and Exo-F) were injected at a controlled flow rate, and their interactions with the cell surface were monitored through response unit (RU) values by changes in the SPR angle.

Cellular uptake assay

Uptake qualitative assays of FITC-loaded exosome samples were examined in concentration-dependent and time-dependent manners. In this regard, 1×10^5 cells were cultured on glass coverslips in each well of 6-well plates under standard conditions. After 24 h, the cells were treated with increasing concentrations of exosomes (15, 30, 60 and 120 µg) for 3 h, as well as for increasing incubation times (30, 60, 120 and 180 min) using 120 µg exosomes under light-protected conditions. After washing with PBS and staining with DAPI (2 µg/mL, Sigma) for 30 min, the treated cells on the glass coverslips were examined by confocal microscopy (BX51, Olympus, Japan). For quantitative evaluation of cellular internalization, cultured and treated cells under the same

conditions as the qualitative assays were trypsinized, collected, and resuspended in a final volume of 500 µL PBS. The fluorescence intensity of the cells was then analyzed using a flow cytometer (BD FACSCalibur, USA) and plotted using FlowJo software (version 10). Furthermore, cellular uptake in non-cancerous cell lines (HUVEC and HFF2) was evaluated both quantitatively and qualitatively at the highest concentration and the longest incubation time.

Drug release study

To simulate and compare the pH- and temperature-dependent release behavior of Dox-loaded exosomes (Exo@Dox and Exo-F@Dox), the Dox release profile was evaluated using a dialysis method in PBS buffers at two pH values (5.5 and 7.4) and two temperatures (37 ˚C and 40 ˚C). To this end, 1000 µL of Dox-loaded exosomes (30 µg/mL exosomal protein), suspended in PBS supplemented with 10% FBS, was placed into a cellulose dialysis bag (MWCO 14 kDa) and immersed in 50 mL of PBS (pH 5.4 or 7.4) under continuous shaking at 37 ˚C or 40 ˚C. At predetermined time intervals (1, 4, 8, 24, 48, and 72 h), 1 mL of the surrounding release medium was collected and analyzed using a UV-vis spectrophotometer at a wavelength of 490 nm to determine the amount of released Dox. An equal volume of fresh PBS was then added to the release medium. The following equation was used to calculate the percentage of Dox-released:

$$\text{Drug release}(\%) = \frac{\sum \text{èt}\left(\text{Amount of drug in release medium at time t}\right)}{\text{Total amount of drug loaded in nanocarrier}} \times 100$$

Eq. 5

In vitro cytotoxicity study

In summary, to estimate the viability of cells exposed to different exosome formulations, MDA-MB-231 (cancerous), HUVECs, and HFF2 (non-cancerous) cell lines were used. In this regard, 2×10^4 cells were seeded in each well of 96-well culture plates and incubated under standard conditions for 48 h. Subsequently, the cells were treated with decreasing concentrations of different exosome formulations (30 µg /mL exosomal protein) and Dox (4.6 µg/mL), including control, Dox, Exo, Exo@Dox, Exo-F, Exo-F@Dox, for 48 h. After the treatment period, 200 µl MTT solution (2 mg/mL in culture medium) was added to each well and incubated under standard conditions in the dark for 4 h. Thereafter, the MTT-containing medium was removed, and 100 µL DMSO was added to each well. After incubation in the dark for 15 min to dissolve the formazan crystals, the optical absorbance was measured at 570 nm using a multimode microplate reader (Biobase, Immuno Scan ELISA Reader). Each experimental group was tested in triplicate.

Migration assay

MDA-MB-231 cells were cultured for 48 h and treated with different groups of exosomes and Dox, including control, Dox, Exo, Exo@Dox, Exo-F, Exo-F@Dox, and Dox-loaded formulations, for 24 h. After trypsinization,1×10^4 cells suspended in 500 µL of DMEM supplemented with 2% FBS were seeded into the insert of a Transwell chamber plate equipped with an 8 µm polycarbonate membrane and incubated for 24 h. Cells that migrated into the lower chamber were stained with methylene blue. Finally, the number of stained cells in each well was counted in ten random fields. This assay was performed in triplicate for each group.

Mitochondria exclusion capacity

Continually, MDA-MB-231 cancer cells treated with various groups of exosomes and Dox were trypsinized and centrifuged. The cellular pellets were incubated with 100 µL of Rhodamine 123 dye (10 µg/mL) for 2 h. The cell suspension was then centrifuged at 2000 × g for 5 min, and the resulting cell pellet was washed three times with 1 mL PBS (pH 7.4), with centrifugation between each washing step, to remove unabsorbed rhodamine dye. Finally, the cells were resuspended in 500 µL of PBS, and 50 µL 4% paraformaldehyde was added to fix the cells. The samples were then analyzed by flow cytometry to evaluate the dye exclusion capacity of different treatment groups at a wavelength of 550 nm.

PCR array analysis

PCR array analysis was employed to study the expression of genes involved in epithelial-mesenchymal transition (EMT) signaling pathways. MDA-MB-231 cells were treated for 24 h with different exosome groups, including control, Dox, Exo, Exo@Dox, Exo-F, Exo-F@Dox, and Dox-loaded formulations (30 µg /mL exosomal protein and 4.6 µg/mL Dox). The treated cells were lysed, and total RNA was extracted using a Trizol Reagent RNA extraction kit (Cat. No. 302-001; RiboExLs). The purity of RNA samples was evaluated using a NanoDrop system (Thermo Fisher, USA). The extracted RNA was then reverse-transcribed into cDNA using Parstous reverse transcription kit (Cat. No. A101162). Subsequently, the expression profiles of EMT-related genes were analyzed using the Human EMT RT^2 Profiler PCR Array (Cat. No. PAHS-084Z; Qiagen GeneGlobe) and a LightCycler 480 Instrument II (Roche). The obtained data were analyzed using the $2^{-\Delta\Delta CT}$ method to calculate relative changes in gene expression associated with the EMT pathway. In this study, a transcriptional change greater than two-fold was considered as the cutoff value, and each experimental group was analyzed in triplicate.

In vivo biodistribution study

The biodistribution of the formulated exosomes was evaluated when the average tumor volume reached approximately 50 mm^3. Since, IC50 of Dox is around 5-10 mg/kg, so we chose 5mg/kg for our study.[40] Subsequently, 100 µg (5 mg/kg) of Exo@Dox, Exo-F@Dox, and free Dox (at two concentrations: therapeutic dose (TD) and the dose loaded in exosomes were injected intraperitoneally into 4T1 tumor-bearing mice, taking advantage of the

inherent fluorescence of Dox. In addition, rhodamine-loaded pristine Exo and Exo-F were used to evaluate the biodistribution profile (n = 3). It is noteworthy that the rhodamine loading procedure for exosomes was the same as that used for Dox loading. After 72 h post-injection, the mice were euthanized, and major organs, including the heart, liver, spleen, lung, and kidney, as well as tumors, were excised and imaged using Kodak In-Vivo Imaging System FX Pro (Kodak, US).

Statistical analysis

All experiments were performed in triplicate. Statistical analyses were conducted using one-way ANOVA (GraphPad Prism 8.4.0) or Microsoft Excel 2019. A P value < 0.05 was considered statistically significant.

Results

Extraction and characterization of exosomes

Recognition of the common exosomal protein markers CD63, CD9, and CD81 by western blot analysis confirmed the successful extraction of exosomes from MDA-MB-231 cell culture (Fig. 1A). Systematic characterization of the exosomes was performed in terms of size, zeta potential, morphology, and structural changes. The hydrodynamic diameter and zeta potential of extracted bulk exosomes were 85.5 nm and −10.3 mV, respectively. After F-protein conjugation, the size and zeta potential of the modified exosomes (Exo-F) changed to 320 nm and -4.5 mV, respectively. Meanwhile, loading of Dox into the extracted exosomes (Exo@Dox) resulted in shifts in size and zeta potential to 175 nm and -6.7 mV, respectively. In addition, loading of Dox into the F-protein-conjugated exosomes (Exo-F@Dox) demonstrated an increase in size and zeta potential to 340 nm and 0.2 mV, respectively (Fig. 1B, 1C). Furthermore, morphological analysis using SEM and TEM confirmed spherical and elliptical shapes for all exosomal groups. Consistent with the DLS results, SEM images exhibited average size of 60.4 nm for Exo, 92.3 nm for Exo@Dox, 112.2 nm for Exo-F, and 151.0 nm for Exo-F@Dox. In addition, TEM images revealed a loss of the cup-shaped structure of exosomes following F-protein conjugation (Figs. 1D, 1E, 1F).

Generally, the FTIR spectra of Exo-F and Exo groups were similar, as recorded in the range of 4000-500 cm^{-1} (Fig. 1G). Regarding protein-associated peaks in the range of 1700-1472 cm^{-1}, more prominent peaks at 1646 cm^{-1} (corresponding to amide I) and 1545 cm^{-1} (corresponding to amide II) were observed in the Exo-F group compared to the Exo group, confirming a higher protein content in the modified exosomes. In addition, FTIR spectra in the ranges of 2922-2853 cm^{-1} and 1491-1448 cm^{-1} confirmed the presence of lipids in both groups. Based on result, by adding F-protein to the surface of exosomes, the surface lipid bonds diminish due to presence of complicated F-protein structure (different kinds of chemical bonds in the protein structure). Furthermore, the Exo group showed higher absorbance peaks than the modified group, reflecting the predominant lipidic structure of the Exo group. Furthermore, signals in the range of 1200 - 900 cm^{-1} were associated with nucleic acids and carbohydrates in both groups. Based on the results, peaks at 1072 $cm^{-1}$and 1156 cm^{-1} in the Exo group were more prominent than those in the Exo-F group, probably due to surface coverage by F-protein in the modified exosomes (Fig. 1G).[41,42] Ultimately, in confirmation of the NMR results, the peak at 1243 cm^{-1}, related to stretching of the aromatic ester carbonyl group, decreased after attachment of the F-protein (Figure 1 H). Next, to validate F-protein conjugation on the exosomes (Exo-F), the samples were investigated by nuclear magnetic resonance (NMR) analysis. As depicted in (Fig. 1E), shifts in the particles' average size distribution led to variation in the peaks of the NMR spectra. The obtained results indicated a slight shift from 62.59 to 69.74 ppm following conjugation of the F-protein with the exosomes. In addition, the reduction of some peaks in the range of 0.75–3.75 ppm indicated changes related to amide and methyl groups. Furthermore, as a result of F-protein conjugation onto the exosomes, a decrease in the peak at 8.4 ppm and the appearance of a new peak at 7.06 ppm were observed, which were attributed to a reduction in aromatic groups and an increased in tyrosine residues, respectively (Fig. 1G). Overall, FTIR and NMR analyses confirmed the successful conjugation of F-protein onto exosomes (Exo-F) (Fig. 1G, 1H). In agreement with the SEM and DLS results, AFM analysis also showed increased size and condensation of Exo-F compared with the Exo group. Topographic imaging of Exo and Exo-F by AFM further confirmed the alterations in the three-dimensional (3D) surface structure between Exo-F and Exo groups (Supplementary file 1).

F-protein coupling and drug loading efficiency

Evaluation of UV-visible analysis illustrated that the encapsulation efficiency of Dox into Exos and Exo-F via the sonication method was 33,2% and 27.3%, respectively. Meanwhile, the loading capacity percentage (LC%) of Exos was determined to be 5.1% for Exo and 4.2% for Exo-F at room temperature. It was calculated that the content of Dox in the exosomes (4.6 µg/mL in sink media) was about 1.53 µg/mL and 1.26 µg/mL for Exo and Exo-F, respectively. Summarily, Table 1 indicates a comparison of EE% and LC% of Dox before and after efficient bioconjugation of F-protein. Also, the quantification reports of relative BE% and BC% of F-protein on the surface of exosomes via covalent binding induced by the EDC-NHS method were determined to be about 81.14% and 31.5%, respectively (Table 1).

In vitro profile of dox release

In this work, the Dox-release behavior of Exo-F and Exos groups was quantified in a pH- (pH 7.4, pH 5.5) and temperature- (37 °C, 40 °C) dependent manner (Eq. 5). Results showed that 60% of Dox was released from Exos-F@Dox at pH 5.5 and 40 °C after 4 h, which was significantly higher than the release rate of Exos-F@

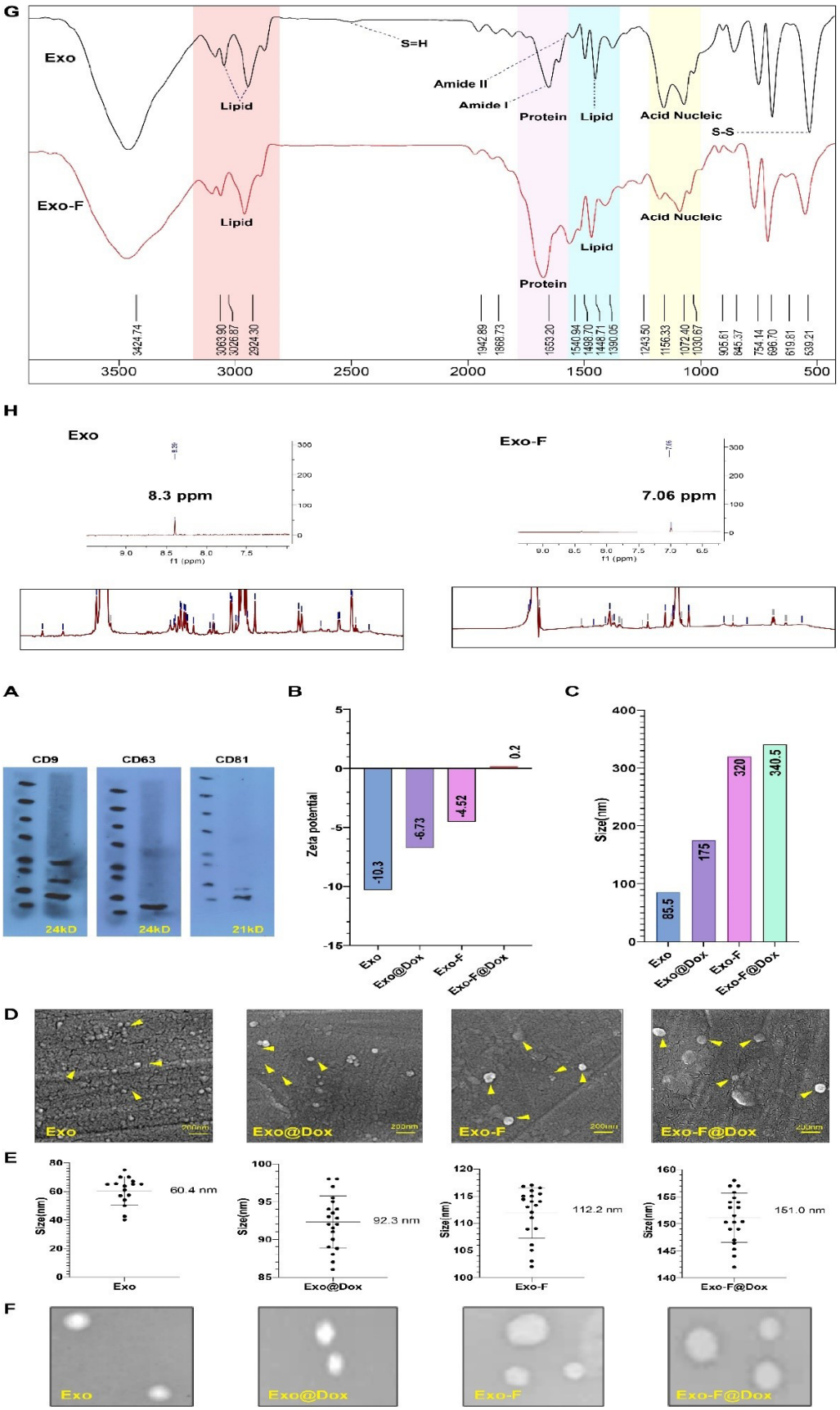

Fig. 1. Physicochemical characterization of different nano-formulated exosome groups: exosome (Exo), Dox-loaded exosome (Exo@Dox), F-protein-conjugated exosome (Exo-F). Dox-loaded F-protein-conjugated exosome (Exo-F@Dox). Western blot analysis confirming the presence of exosomal biomarkers (CD9, CD63, and CD81). **(B)** Comparison of the zeta potential of Exo, Exo@Dox, Exo-F, and Exo-F@Dox. **(C)** Shifts in the hydrodynamic diameter of Exo, Exo@Dox, Exo-F, and Exo-F@Dox determined by DLS analysis **(D)** Morphological imaging of the Exo, Exo@Dox, Exo-F, and Exo_F@Dox by scanning electron microscope (SEM). **(E)** Size analysis of Exo, Exo@Dox, Exo-F, and Exo-F@Dox based on SEM microscope (n = 100; mean ± SD). **(F)** Transmission electron microscopy (TEM) images of Exo, Exo@Dox, Exo-F, and Exo-F@Dox. **(G)** Characterization of the surface morphology of Exo and Exo-F groups by FTIR spectra, **(H)** the complete NMR spectra of Exo and Exo-F groups.

Dox at pH 7.4 and 37 °C (17%), and Exo@Dox at pH 5.5 and 40 °C (22%) and at pH 7.4 and 37 °C (18.2%). Also, a controlled release behavior was observed in the Exo-F group at pH 5.5 and 40 °C over the following 48 h, compared to the other groups. This phenomenon confirmed the positive synergistic effect of acidic pH and elevated temperature on the release of Dox from Exos-F@Dox, compared to each group condition alone (Fig. 2A).

Surface plasmon resonance (SPR) confirmed increased interactions by Exo-F

Comparison of the sensograms of the Exo-F and Exo interactions with the MDA-MB-231 cells membrane exhibited an increase in RU (resonance units) signal up to four times higher for Exo-F than Exo at the same concentration (30 µg/mL exosomal protein), indicating enhanced interaction of EXO-F with MDA-MB-231 cancer cells (Fig. 2B).

Modified exosomes (Exo-F) showed increased uptake in MDA-MB-231 cells

The efficiency of cellular uptake of FITC-loaded exosomes by MDA-MB-231 cells was assessed both qualitatively and quantitatively, using fluorescent microscopy and flow cytometry, respectively. Results showed that fluorescently labeled exosomes were internalized by the cells in a time- and concentration-dependent manner, highlighting significantly higher internalization of modified exosomes (Exo-F) compared to non-modified exosomes (Exo) in MDA-MB-231 cells (Fig. 3). In contrast, non-cancerous cell lines, HUVEC and HFF2, demonstrated significantly lower cellular internalization than cancer cells, both for the modified and non-modified formulations (Fig. 4).

Cytotoxicity of different groups of exosomes in MDA-MB-231, HUVEC, and HFF2 cells

In-vitro cytotoxicity studies of different groups, including free Dox, Exo, Exo@Dox, Exo-F, Exo-F@Dox, F-protein, and control, indicated that loading of Dox into Exo-F significantly decreased the IC50 concentration after 48 h of incubation. The IC50 value for Dox loaded in Exo-f@Dox formulation was 0.19 µg/mL of Dox concentration, whereas the Exo@Dox formulation did not reach an

Table 1. The properties of binding and loading of exosomes

Efficiency	Samples		
	Unmodified exosomes (Exo)	Modified exosomes (conjugated F-protein exosomes) (Exo-F)	Formula
Loading capacity (LC%)	5.1%	4.2%	Eq. 1
Encapsulation efficiency (EE%)	33,2%	27.3%	Eq. 2
Binding capacity (BC%)	-	31.5%	Eq. 3
Binding efficiency (EE%)	-	81.14%	Eq. 4

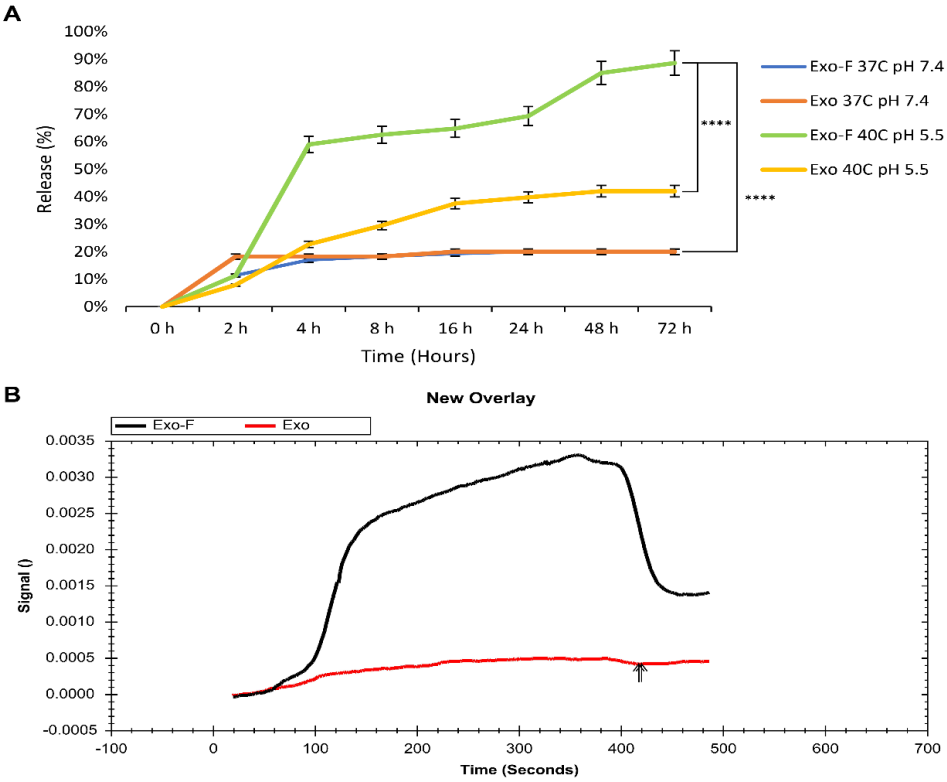

Fig. 2. (A) In vitro drug release profile of Dox from Exo and Exo-F groups over 72 h under different conditions: pH 7.4 and pH 5.5, at 37 ˚C and 40 ˚C. Data are presented as mean ± SD, n = 3, ****P < 0.0001. **(B)** SPR analysis of surface interaction of Exo and Exo-F groups with MDA-MB-231 cells.

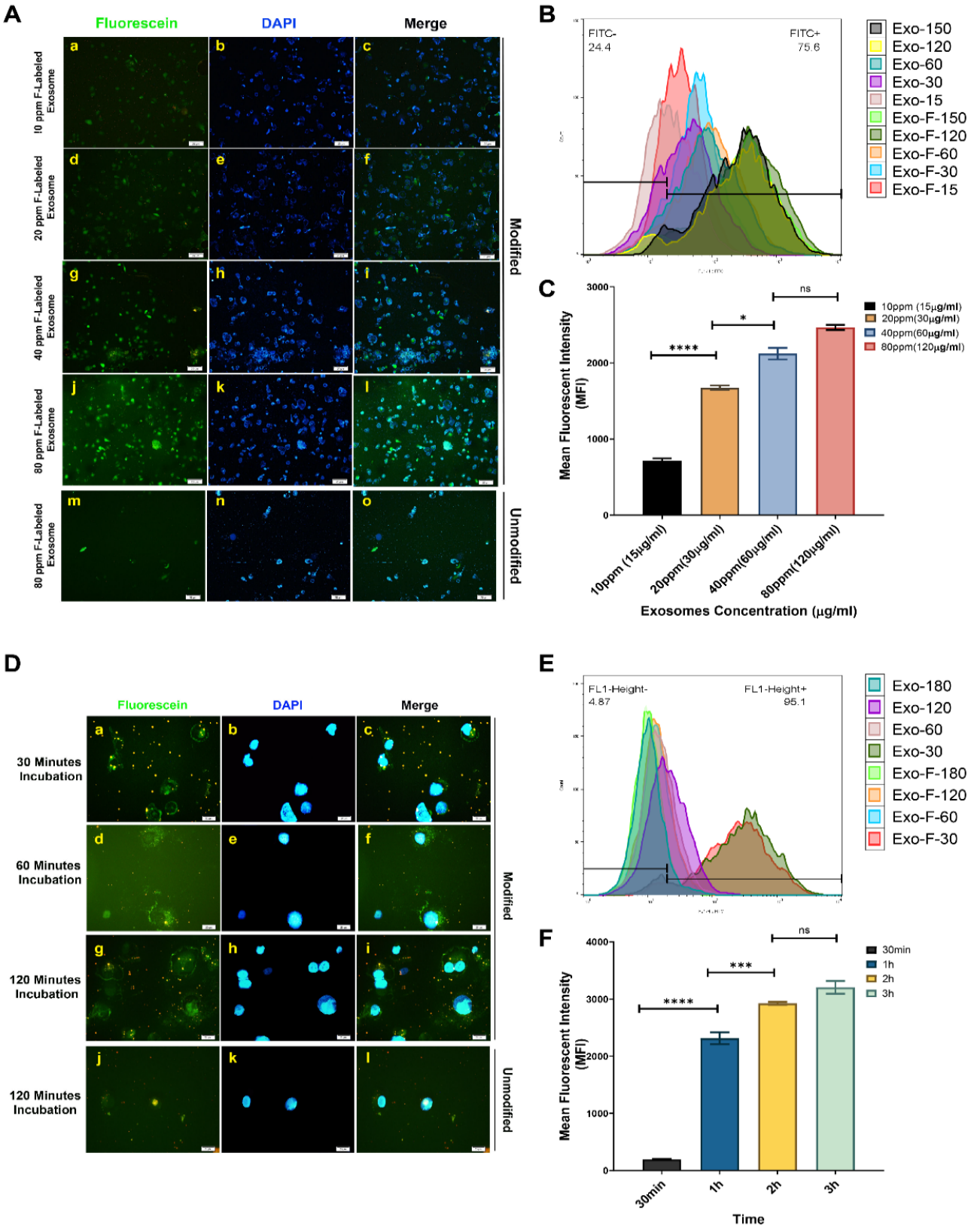

Fig. 3. In vitro concentration-dependent cellular uptake in MDA_MB-231 cells. **(A)** Qualitative concentration-dependent uptake of different formulations of FITC-loaded exosomes: Exo@FITC (m-o) and Exo-F@FITC (a-j) at concentrations of 15, 30, 60, and 120 μg/mL of exosomal protein with an exposure time of 3 h in MDA_MB-231 cells, assessed by fluorescence microscopy. **(B)** Quantitative concentration-dependent uptake of Exo@FITC and Exo-F@FITC at the same concentrations and exposure time in MDA_MB-231 cells, measured by flow cytometry. **(C)** Calculation of the mean fluorescence intensity (MFI) of Exo-F@FITC at 15, 30, 60, and 120 μg/mL in MDA_MB-231 cells. In vitro time-dependent uptake of different formulations of FITC-loaded exosomes in MDA_MB-231 cells. **(D)** Qualitative time-dependent uptake of Exo@FITC (J–L) and Exo-F@FITC (a–j) at 30, 60, and 120 min with 120 μg/mL of exosomal protein, assessed by fluorescence microscopy. **(E)** Quantitative-time-dependent uptake of Exo@FITC and Exo-F@FITC at 30 min, 60 min, 120 min with 120 μg/mL of exosomal protein, measured by flow cytometry. **(F)** Calculation of the mean fluorescence intensity (MFI) of Exo-F@FITC at 30 mi, 60 min, 120 min with 120 μg/mL of exosomal protein in MDA_MB-231 cells. Data are presented as mean ± SD, n = 3, * $P < 0.1$, *** $P < 0.007$, and **** $P < 0.0001$.

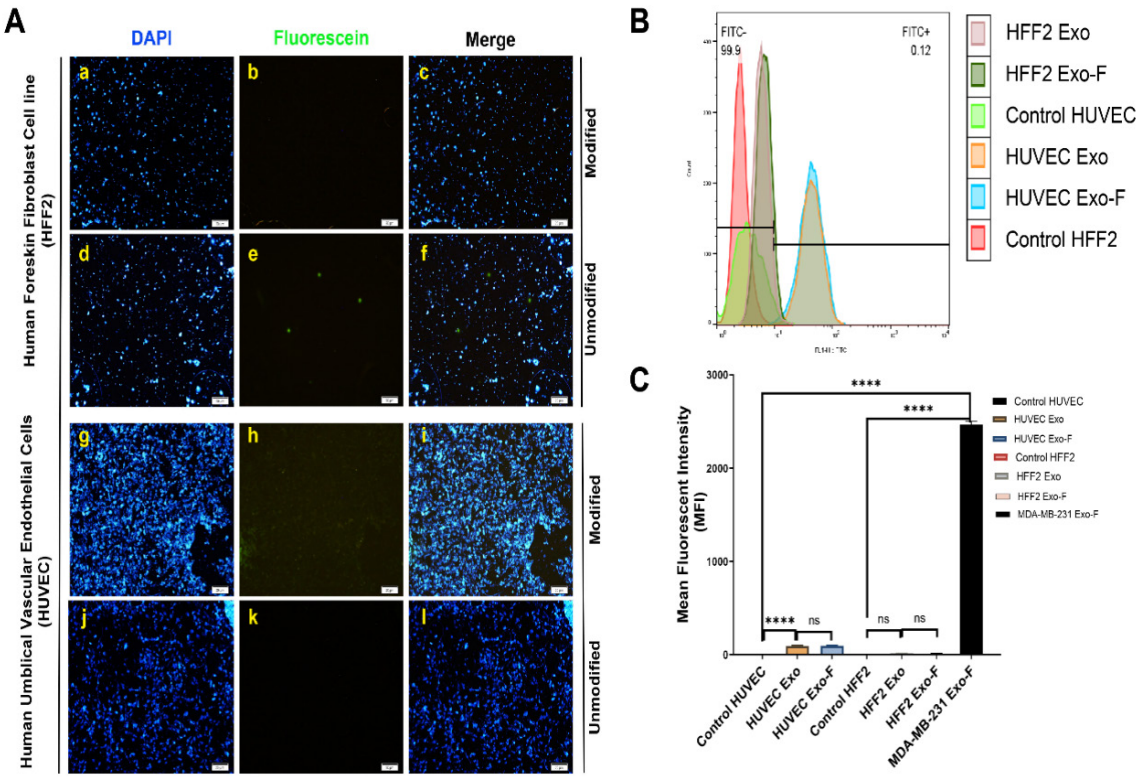

Fig. 4. In vitro cellular uptake in HUVEC and HFF2 cells. **(A)** Qualitative uptake of different formulations of FITC-loaded exosomes: Exo@FITC (a–c) and Exo-F@FITC (d–f) at 120 min and 120 μg/mL of exosomal protein, assessed by fluorescence microscopy. **(B)** Quantitative uptake of Exo@FITC and Exo-F@FITC at 120 min and 120 μg/mL of exosomal protein in HUVEC and HFF2 cells, measured by flow cytometry. **(C)** Calculation of the mean fluorescence intensity of Exo@FITC and Exo-F@FITC at 120 min and 120 μg/mL of exosomal protein in HUVEC and HFF2 cells. Data are presented as mean ± SD, n = 3, **** $P < 0.0001$.

IC50 at the loaded Dox concentration (1.53 μg/mL). The IC50 value for free Dox was 4.6 μg/mL. According to our findings, F-protein-functionalized exosomes exhibited 24.2-fold stronger cytotoxicity than free Dox and even Exo@Dox (Figure 5 A). Interestingly, Dox-free Exo-F showed higher cytotoxicity in MDA-MB-231 cells compared to HUVEC and HFF2 cells (Figure 5 B,). which strongly suggests investigating the underlying mechanism in future studies. A comparison of IC50 values for the different exosome groups on MDA-MB-231, HUVEC, and HFF2 cells, as determined by MTT assay, is summarized in Table 2.

Exosomes conjugated to f-protein decrease migration of MDA-MB-231

Results of migration assay illustrated that cells treated with Exo-F@Dox, Exo-F and free Dox (at its IC50 concentration) exhibited a marked lost their migratory capability compared to other formulations. As expected, treatment with free Exo significantly enhanced the migratory properties of cancer cells compared to the control group, indicating the natural role of cancer-derived exosomes in promoting metastasis. More interestingly, Exo@Dox showed at least a threefold greater inhibition of migration compared to Exo (30% vs. 10%), highlighting the potency of released Dox in counteracting the stimulatory effects of free exosomes on cellular migration (Fig. 6A).

PCR array analysis

The effect of surface modification of exosomes with F-protein on the EMT machinery was assessed using PCR array analysis. Our results indicated that conjugation of RSV F-protein to the exosome surface induced shifts in the expression patterns of genes involved in the classical EMT process compared to other exosomal groups. The data confirmed that MDA-MB-231 cells treated with Dox, Exo, and Exo@Dox exhibited a Dox-resistant, EMT-activated phenotype, with upregulation of EGFR, Akt, WNT, MMP2, TGFβ2, ESR1, SERPINE1, and Notch-1 adaptors by more than 2-fold (Fig. 6B).[43,44]

Considering the role of MMP9 in promoting EMT,[45,46] no significant differences were observed in MMP9 expression among all treated groups. Additionally, given the role of CDH1 in maintaining epithelial characteristics.[47,48] Results showed that CDH 1 expression in cells treated with modified exosomes (Exo-F, Exo-F@Dox groups) was slightly decreased compared with other treated groups, but not significantly. In contrast, cells treated with Exo, Exo-Dox, and free Dox showed a significant increase in CDH 1 expression. Meanwhile, CDH 2, a mesenchymal marker, showed a significant increase in the group treated with free Dox and a very pronounced decrease in Exo-F group. Examination of COL4A1 expression revealed a significant increase in all groups except Exo-F. Interestingly, contrary to expectations, vimentin (Vim) expression was significantly increased in the Exo-F group compared to the other groups (Fig. 6B).

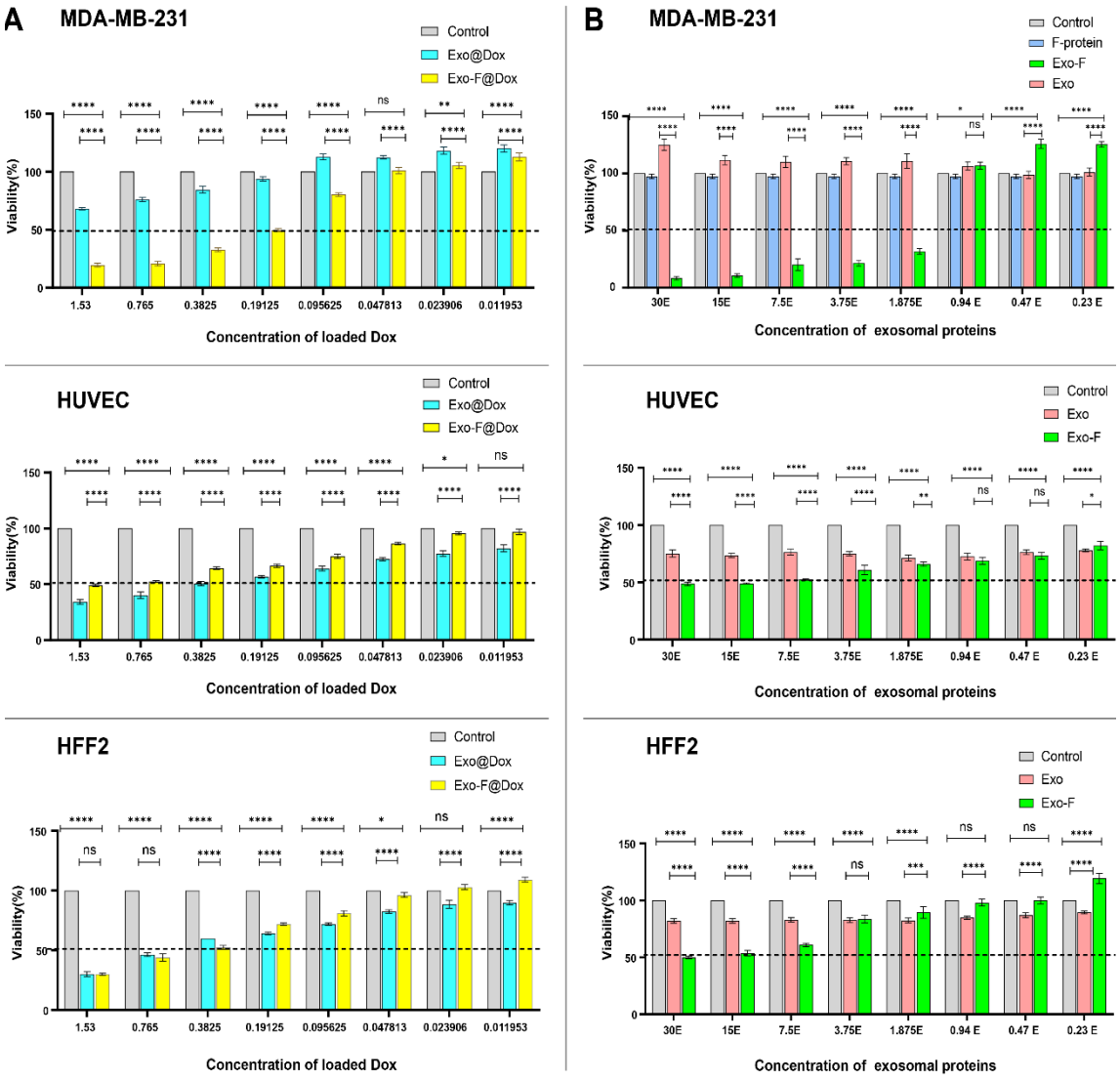

Fig. 5. Comparison of in vitro cytotoxicity in MDA-MB-231, HUVEC-, and HFF2 cells using the MTT assay after 48 h treatment with different groups, including: control, free Dox (Dox), Exo alone (Exo), F-protein (F), Dox-loaded exosome (Exo@Dox), F-protein-conjugated exosomes (Exo-F), Dox-loaded F-protein-conjugated exosomes (Exo-F@Dox). **(A).** Cell viability of MDA-MB-231, HUVEC-, and HFF2 cells treated with different doses of Dox (1.53, 0.76, 0.38, 0.19, 0.095, 0.048, 0.023, and 0.011 µg/mL). **(B)** Cell viability of MDA-MB-231, HUVEC-, and HFF2 cells treated with different doses of exosomal protein (30, 15, 7.5, 3.75, 1.87, 0.94, 0.47, and 0.23 µg/mL). Data are presented as mean ± SD, n = 3, analyzed by 2-way ANOVA. ns < 0.05; * P < 0.01, ** P < 0.006, *** P < 0.0008; **** P < 0.0001.

Table 2. Comparison of IC_{50} values of different exosome groups in MDA-MB-231, HUVEC, and HFF2 cells determined by MTT assay

Cells	Sample	Doxorubicin	Free F-protein	Exosomes	Dox loaded exosomes	F-protein modified exosomes loaded Dox	F-protein modified exosomes
	Abbreviation	Dox	F-protein	Exo	Exo@Dox	Exo-F@Dox	Exo-F
MDA-MB-231	IC50 based of Dox concentration	4.6µg/mL	-	Increase the viability	Not seen for Dox loaded (need to the high concentration of Dox	0.19 µg/mL of Dox concentration	-
	IC50 based of exosomes concentration	-	Not change	Increase the viability	-	-	0.1 µg/mL of exosomal protein concentration
HUVEC	IC50 based of Dox concentration	4.6µg/mL	-	Not change	0.38 µg/mL of Dox concentration	1.53 µg/mL of Dox concentration	-
	IC50 based of exosomes concentration	-	-	Not change	-	-	30 µg/mL of exosomal protein concentration
HFF2	IC50 based of Dox concentration	4.6µg/mL	-	Not change	0.70 µg/mL of Dox concentration	0.38 µg/mL of Dox concentration	-
	IC50 based of exosomes concentration	-	-	Not change	-	-	30 µg/mL of exosomal protein concentration

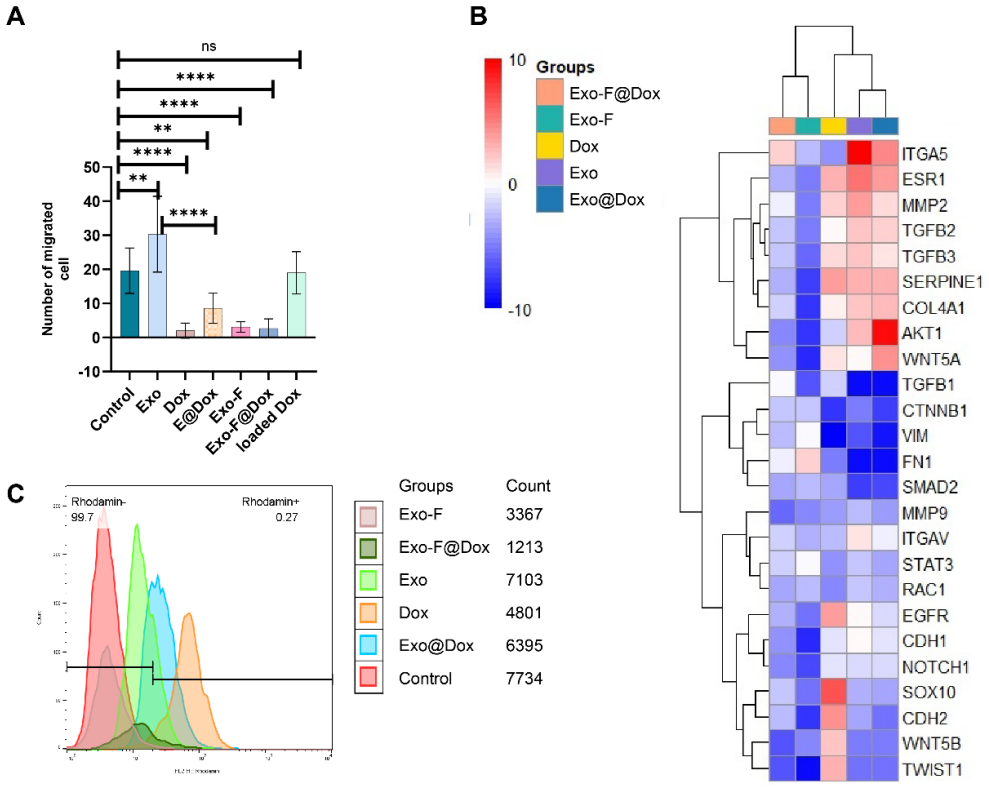

Fig. 6. **(A)** Migration assay using Transwell inserts. Monitoring MDA-MB-231 cell migration after 48 h of treatment with Control, Exos, Dox, Exo@Dox, Exo-F, and Dox-loaded Exo-F@Dox, n = 10; ** $P < 0.005$, and **** $P < 0.0001$. **(B)** Clustergram illustrating genes involved in the EMT pathway in MDA-MB-231 cells treated with Dox, Exos, Exo@Dox, Exo-F, and Exo-F@Dox for 48 h (n = 3). Red areas indicate upregulation, and blue areas indicate downregulation. **(C)** Monitoring mitochondrial membrane potential (ΔΨm) in the MDA-MB-231 cells treated by Control, Dox, Exo, Exo@Dox, Exo-F, and Exo-F@Dox, assessed by flow cytometry.

Modified Exos (Exo-F, Exo-F@Dox) induce mitochondria extrusion

To evaluate mitochondrial membrane integrity and negative membrane potential (ΔΨm), rhodamine-123 was used.[49] Flow cytometry analysis was then employed to quantify mitochondrial membrane integrity in cells treated with different exosome groups, including Control, Exo, Dox, Exo@Dox, Exo-F, and Exo-F@Dox. The results showed that cells treated with Exo-F and Exo-F@Dox demonstrated mitochondrial dysfunction and increased extrusion of rhodamine-123 (Fig. 6C).

In vivo biodistribution study

An in vivo biodistribution study was conducted in female 4T1 tumor-bearing Balb/c mice to evaluate exosomes accumulation in various organs (Fig. 7A). Our results confirmed that around 17 µg (5.8 folds lower than TD) and 15.7 µg (6.4 folds lower TD) for pristine and modified Exo, respectively. Worth mentioning, these amounts of Dox was loaded into 30 µg exosomal protein content, which injected to each mouse. Ex vivo imaging results showed that, 72 h post-injection, rhodamine-labeled Exo-F successfully accumulated at the tumor site and in the brain. In contrast, Exo-F@Dox was primarily entrapped in the liver in addition to the brain and tumor. Interestingly, rhodamine-loaded Exo was distributed across all organs except the spleen and lung (n = 3) (Fig. 7A) Moreover, tumor volume measurements confirmed inhibition of tumor growth and a significant decrease in tumor size in the groups treated with Exo-F and Exo-F@Dox; over 10 days (n = 3) (Fig. 7B).

Discussion

Considering the drawbacks of chemotherapeutic agents such as Dox, and their insufficient bioavailability due to elimination via P-glycoproteins, the effectiveness of chemotherapy has been far from satisfactory.[50] Recently, many efforts have focused on expanding the application of exosomes as biocompatible carriers for the delivery of chemotherapeutic agents such as Dox.[51] Despite the advantages of pristine exosomes, the use of natural exosomes as carriers and as targeted therapeutic or diagnostic platform has demonstrated considerable limitations, particularly in targeting ability.[27,52] Moreover, specific targeting of cancer cells seems to be crucial for the development of effective therapeutic agents.[53] Herein, we confirmed that RSV F-protein -modified MDA-MB-231 cell-derived exosomes could potentially be used for targeting TNBC breast cancer.

Physicochemical characterization of exosomes isolated from MDA-MB-231 cells demonstrated their authenticity, morphology, and structural properties using different techniques. These properties proved that the isolated exosomes possess suitable features for drug delivery applications.[54] However, as noted earlier, due to the presence of different functional proteins on their surface, pristine exosomes lack targeting specificity.[12] Consistent with other experimental studies, alterations in the

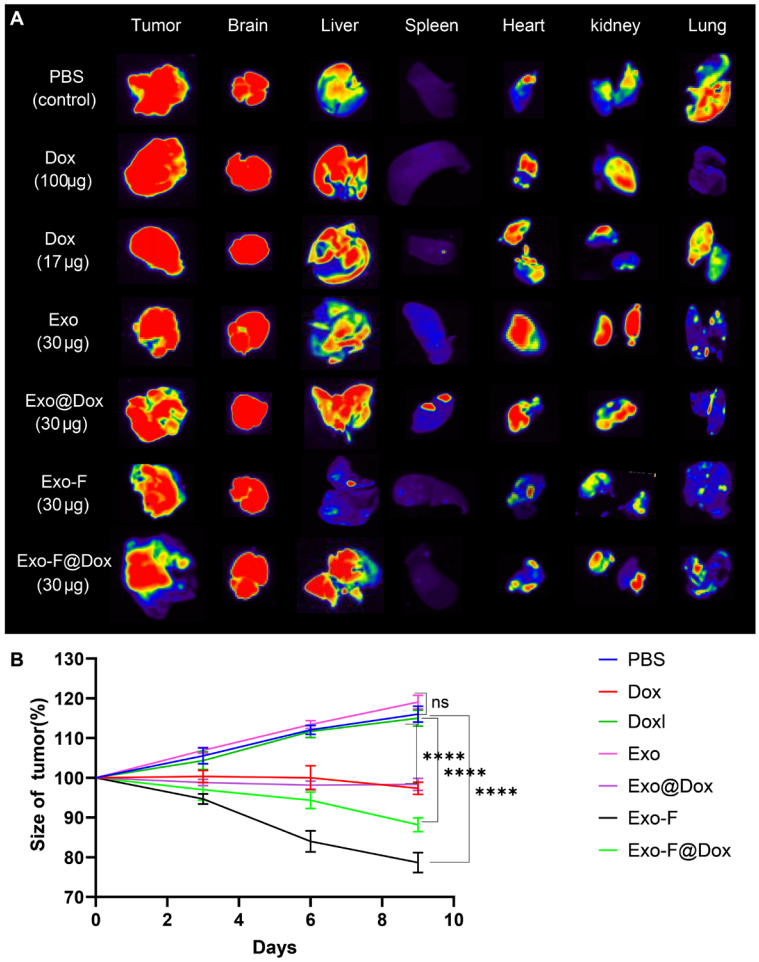

Fig. 7. In vivo biodistribution study of different exosome formulations and tumor size. **(A)** Ex vivo imaging of major organs, including heart, kidney, lung, liver, spleen, brain, and tumor, after administration of Dox-loaded groups (Dox at TD, Dox-loaded Exo@Dox, and Exo-F@Dox) and rhodamine-stained groups (Control, Exo, and Exo-F). Mice received three injections over 10 days, and imaging was performed 72 h after the last injection. **(B)** Tumor volumes in mice treated with PBS, Dox (at TD), Dox-loaded, Exo, Exo@Dox, Exo-F@Dox, and Exo-F over 10 days ($P<0.0001$; n = 3).

physicochemical properties of the isolated exosomes confirmed the successful attachment of F-protein onto the exosomes surface.[55] Also, FTIR results confirmed the successfully attachment of RSV F-protein to the surface of harvested exosomes, via covalent bond. As drug molecules could be found in the exosome's cavity or on the surface of them, obviously hydrodynamic and real size of exosomes would be altered after the loading procedure. Therefore, changes in the zeta potential and size of exosomes are referred to drug loading in nano-pharmaceutical experiments. Since, DLS results are equal to 10^6 times of reflected laser beam from nano sized entities size. In fact, any aggregation would be shown as a big curve in harvested peaks. Also, we should keep in mind that the reported size by DLS is hydrodynamic diameter of particles not their real size that can be seen in SEM or TEM, especially unexpected increase in the size of exosomes after modification by F-protein. Therefore, modification of particles by any agent which attracts higher solution around the particle, resulted in larger size than its real size depends on concentration of that agent on the particle surface. In contrast to the drug loading procedure in other types of nanoparticles (encapsulation or attachment of drug to the structure of nanoparticles), loading into highly compacted structure of exosomes need to relatively and transient instability of exosomes membrane using sonication or other physicochemical routs. Obviously, increasing the stability of exosomes membrane by addition of F-protein, decrease the efficacy of sonication method for drug loading procedure. On the other hand, enhance the power of sonication for compensation the mentioned problem was not working, because it causes to disruption of exosomes integrity. Therefore, LC% and EE% in this study maintained in a narrow range between pristine and modified exosomes. Also, drug releasing kinetic in the cells and their following endosomal escape efficacy is the most important level in any drug delivery discipline. In the case of cancerous cells, the pH of lysosomes is around 4.5-5 and intratumorally temperature is around 40-45 °C, while these parameters are 5.5-6 and 37 °C in normal tissues, respectively.[56] Therefore, the drug release profile of any nano systems should be controlled in these circumstances for checking treatment regimen and possible undesired side effects in normal cells. Importantly, due to the indisputable effect of proteins on the stability of lipid-derived nanoparticles (exosomes are like to immunoliposomes structurally) we added 10% albumin to release media for more exact

simulation of biological media.[57] In addition to changes in the physicochemical properties of exosomes, our cellular internalization studies verified more efficient functionalization of exosomes in a time- and concentration-dependent manner.[58,59] As higher interaction and internalization of carriers are directly related to improved therapeutical outcomes, functionalizing of exosomes by F-protein caused to achieving this goal. Also, specific targeting resulted in lower drug-related side effects and reduced undesired nano-bio interactions.[12] Importantly, the internalization of the Exo-F formulation was lower in non-cancerous HUVEC and HFF2 cells. Obviously, the lower internalization of Exo-F in non-cancerous cells occurred due to lower expression of F-protein -specific receptors on these cells and their higher expression on the MDA-MB-231 cells.[60] Additionally, despite the relatively low LC% and EE% compared with some synthetic nanoparticles, the specific internalization of developed F-protein-modified exosomes compensates for the required amounts of exosomes for drug delivery purposes. From a nano-bio interface points of view, the improved performance of nano-based formulations resulted in fewer unwanted effects.[61] In fact, according to the scientific findings over the past three decades, decreasing the number of injected nanocarriers into the body influences off-target effects, side effects, accumulation at the diseased site, and finally the therapeutic index.[26] According to evidence, the attached F-protein targets Nucleolin, IGF1, CD14, and TLR4, which are overexpressed in cancer cells, especially breast cancer cells.[37,62,63] In addition to the targeting behavior of the developed exosomes, the intracellular burst release of Dox from EXoF@Dox formulation occurred in a pH- and temperature-dependent manner, consistent with lysosomal conditions in cancer cells.[27,64] This intracellular burst release, together with the cytotoxic effects of Dox in MDA-MB-231 cells, occurred due to saturation of multidrug resistance (MDR) proteins involved in drug efflux.[64-66] Therefore, sufficient amounts of Dox remain available for DNA adduct formation and induction of single- and double-strand breaks.[67] It is also worth mentioning that the slow release rate of encapsulated Dox from exosomes may present a reasonable explanation for the higher cellular toxicity of free Dox compared with Exo@Dox, as confirmed by other studies.[27] However, contradictory results have been reported by Schindler et al, who confirmed higher in vitro cytotoxicity of the Exo@Dox formulation compared with free Dox.[28] Surprisingly, the modified formulation showed stronger inhibitory effects on the migration ability of MDA-MB-231 cells than the unmodified formulation, consistent with its cytotoxicity effects. Developing a targeted nanoformulation using two natural compound (breast cancer derived exosomes and RSV F-protein) which increase the potency of Dox in eradication of breast cancer tumors not by altering the Dox inherent anti-cancer properties (EMT inhibition is one of Dox usage outcomes),[68] but by lowering needed amounts of drug due to showing enhanced targeting delivery. On the other hand, a great and strange finding of this study was potent anti-tumor effects of F-protein modified exosomes (even EMT signaling inhibition), while none of the portions of developed nanoparticles showed even slightly similar results alone. Unfortunately, due to lack of time and budget we couldn't find exact mechanism of this odd phenomenon, but It seems F-protein modified exosomes follow the same trajectory of Dox in invasive breast cancer. Indeed, results of this study introduced a therapeutic compound that didn't report previously in the literature that need to be unraveled as we proposed in the manuscript already. Possibly, the anti-migratory effects of the modified exosomes can be attributed to the improved anti-oncogenic activity of the F-protein on the surface of the modified exosomes,[69] which should be further investigated through EMT pathway gene expression profiling. Furthermore, emerging evidence suggests an insufficient role of Dox in breast cancer treatment due to the maintenance of stemness of MDA-MB-231 cells[70] and the induction of EMT associated with the development of Dox resistance. It should also be mentioned that the morphological changes observed in Dox-treated MDA-M-231 cells, from spindle-shaped to round-shaped, suggest the promotion of stemness properties in the surviving cells.[64] Moreover, MDA-MB231 cells-derived exosomes primarily act as facilitators of EMT via reprogramming of the EMT pathway.[71] Overall, assessment of the molecular profile of CSCs by PCR array supports the expectation that the proliferation, invasion, and migration properties of CSCs are up- or down-regulated through shifts in cellular adhesion characteristics.[72] Therefore, it can be imagined that Dox-resistant MDA-MB-231 cells are closely associated with promotion of the EMT process and, simultaneously, expansion of stemness properties.[73-75] According to PCR array results, maintenance of stemness properties in CSCs originates from upregulation of the TGF-β, Wnt, Notch, ERK, and Akt signaling pathways.[73] Classical EMT is characterized by downregulation of E-cadherin (an epithelial marker) and upregulation of vimentin (Vim, a mesenchymal marker).[46,47] However, the effects of our formulations on cell migration showed that alterations in several intermediate molecules involved in the EMT pathway led to a shift from the classical EMT pathway toward a mixed or altered EMT state in this study.[45,46] According to the literature, upregulation of Vim and downregulation of E-cadherin following binding of RSV F-protein to the exosome surface (Exo-F and Exo-F@Dox groups) probably occurred through activation of the p38 MAPK pathway-dependent TGF-β/Smad cascade.[76] Overall, TGF-β1, as an EMT-inducing factor, leads to downregulation of E-cadherin (CDH1) in cancer cells.[77] However, in line with our findings, Talukdar et al suggested a robust distribution of E-cadherin in RSV-infected cells, although they were treated with TGF-β1; these results contradict the conventional role of TGF-β1 in the EMT process.[78] This observation suggests that RSV

infection may induce a shift in the classical EMT pathway in infected cells. In conclusion, this phenomenon suggests that the presence of RSV F-protein in the structure of our developed exosomes may change stemness, migration, invasion, and the classical EMT pathway.[77] Interestingly, a significant increase in COL4A1 expression was observed in all groups except the Exo-F group; however, this change did not affect cell migration. Nevertheless, a clear explanation for this behavior could not be identified.[79]

Dysfunction of the mitochondrial membrane potential observed after incubation of MDA-MB-231 cells with Exo-F and Exo-F@Dox is consistent with reports by Funchal et al, which showed that binding of RSV F-protein to TLR4 leads to activation of the Raf/MEK/ERK and P38 MAPK signaling pathways, followed by activation of NADPH oxidase complexes, increased ROS production, and ultimately stimulation of NET release.[5] Changes in ΔΨm provide a reliable indicator for measuring ROS production and analyzing mitochondrial function.[80] Byrd et al also reported that an increase in FN1 (fibronectin) levels confirms the NET release phenomenon through involvement of the ERK/MAPK signaling pathway.[81] Therefore, the groups examined in our study may stimulate cancer cell growth through this mechanism. Furthermore, Fibronectin-TLR4 interaction – one of the main targets of RSV F-protein can induce platelet aggregation and arterial thrombosis, thereby triggering NETosis in cancer.[81] Another key factor in the activation of NETosis is Vim, which was increased in the Exo-F group. Thiam et al confirmed the central role of Vim intermediate filaments in rupturing the nuclear membrane and decondensation of chromatin during NETosis process.[82,83] Moreover, activation of the TAK1/MAPKP38/p53 signaling cascade, following a relative increase of TGFβ1 after exposure to the Exo-F group, is probably mediated by conjugation of F-protein to the TLR4. However, further research is needed to determine the precise signaling pathways activated by RSV F-protein-attached entities. More importantly, the results proved that free F-protein could not exert any toxic effects on tumor in vivo.

Conclusion

In recent decades, considerable attention has been devoted to designing systems for the targeted delivery of cytotoxic drugs to tumor cells without harming surrounding tissues. In this study, we developed a new class of modified exosomes (Exo-F) and Dox-loaded exosomes (Exo-F@Dox), with size and zeta potential in the appropriate range for in vivo distribution, which demonstrated increased cytotoxicity against MDA-MB-231 and TME breast cancer cells. The IC_{50} value of Exo-F@Dox and free Dox after 48 h of exposure were about 0.19 μg/mL and 4.6 μg/mL, respectively, indicating a 24-fold increase in potency ($P < 0.0001$). Besides, the cellular migration assay confirmed reduced migration by the modified exosomes. Surprisingly, Exo-F group showed higher cytotoxicity and greater inhibition of migration than even the Exo-F@Dox group. These effects likely stem from the role of the F-protein in inducing apoptosis and inhibiting the EMT pathway. Additionally, the high surface interaction and enhanced internalization into cancer cells, along with the burst release Dox from the F-modified exosomes, highlight the effective targeting capability of our designed exosomes for breast cancer cells. In vivo imaging studies confirmed that, due to F-protein coupling, the fluorescent distribution to vital organs, including the lung, heart, spleen, and kidney, was dramatically decreased. In this case, the Exo-F@Dox group showed accumulation in the liver due to the enhanced size and hepatic trapping, whereas the Exo-F group showed a dramatic decrease in liver distribution. Overall, the ability to improve targeting efficiency, facilitate drug delivery, and enhance therapeutic efficacy makes F-protein-modified exosomes highly promising for future clinical applications in cancer chemotherapy.

Perspective

Encouraged by our results, F-protein-modified exosomes (Exo-F) represent a promising platform as a superior alternative for cancer treatment, especially for brain cancer, compared to existing approaches. Their precise targeting and efficient accumulation suggest a bright prospect for future cancer chemotherapy. However, to gain deeper insights into the effects and mechanisms of these particles, more detailed studies are warranted.

Acknowledgments

We thank the personnel of the Faculty of Advanced Medical Sciences and the Department of Medical Biotechnology, for their help and guidance. We thank Dr Amir Fattahi for editorial assistance. The authors declare that they have not used AI-generated work in this manuscript.

Authors' Contribution

Conceptualization: Amir Zarebkohan, Reza Rahbarghazi, Morteza Milani, and Mohammad Nouri.
Data curation: Narges Mardi, Hamid Lotfimehr, Mehdi Talebi, Sharareh Khavandkari, Zahra Abbasi-Malati, Cigir Biray Avci, Nastaran Sedghi Samarkhazan, Elham Shahriyari, Asghar Khalilnezhad.
Formal analysis: Narges Mardi and Amir Zarebkohan.
Funding acquisition: Mohammad Nouri, Reza Rahbarghazi.
Investigation: Narges Mardi.
Methodology: Narges Mardi.
Project administration: Amir Zarebkohan and Reza Rahbarghazi.
Resources: Amir Zarebkohan, and Reza Rahbarghazi.
Software: Amir Zarebkohan, Narges Mardi and Reza Rahbarghazi.
Supervision: Amir Zarebkohan, Reza Rahbarghazi and Morteza Milani, and Mohammad Nuori.
Validation: Amir Zarebkohan, and Reza Rahbarghazi.
Visualization: Narges Mardi, Amir Zarebkohan.
Writing–original draft: Narges Mardi.
Writing–review & editing: Amir Zarebkohan, Morteza Milani.

Competing Interests

The authors declare that they have no known competing financial interests or personal relationships that could have appeared to influence the work reported in this paper.

Ethical approval

This study was conducted in accordance with the World Medical Association Declaration of Helsinki. The animal experiments were done in accordance with the guidelines of "The Guide for the Care and Use of Laboratory Animals" (NIH Publication No. 85-23, revised 1996).

Funding
This project was funded by Tabriz University of Medical Sciences (grant number 66627), and ethical approval code IR.TBZMED.VCR.REC.1400.158.

Supplementary files
Supplementary file 1 contains Figs. S1-S3.

References

1. Barbati F, Moriondo M, Pisano L, Calistri E, Lodi L, Ricci S, *et al.* Epidemiology of Respiratory Syncytial Virus-Related Hospitalization Over a 5-Year Period in Italy: Evaluation of Seasonality and Age Distribution Before Vaccine Introduction. *Vaccines (Basel)* **2020**; 8: 15. doi:10.3390/vaccines8010015
2. Chatterjee A, Mavunda K, Krilov LR. Current State of Respiratory Syncytial Virus Disease and Management. *Infect Dis Ther* **2021**; 10: 5–16. doi:10.1007/s40121-020-00387-2
3. Juliana A, Zonneveld R, Plötz FB, van Meurs M, Wilschut J. Neutrophil-endothelial interactions in respiratory syncytial virus bronchiolitis: An understudied aspect with a potential for prediction of severity of disease. *J Clin Virol* **2020**; 123: 104258. doi:10.1016/j.jcv.2019.104258
4. Herbert JA, Deng Y, Hardelid P, Robinson E, Ren L, Moulding D, *et al.* β(2)-integrin LFA1 mediates airway damage following neutrophil transepithelial migration during respiratory syncytial virus infection. *Eur Respir J* **2020**; 56: 1902216. doi:10.1183/13993003.02216-2019
5. Funchal GA, Jaeger N, Czepielewski RS, Machado MS, Muraro SP, Stein RT, *et al.* Respiratory syncytial virus fusion protein promotes TLR-4-dependent neutrophil extracellular trap formation by human neutrophils. *PLoS One* **2015**; 10: e0124082. doi:10.1371/journal.pone.0124082
6. Demkow U. Neutrophil Extracellular Traps (NETs) in Cancer Invasion, Evasion and Metastasis. *Cancers (Basel)* **2021**; 13: 4495. doi:10.3390/cancers13174495
7. Eckardt-Michel J, Lorek M, Baxmann D, Grunwald T, Keil GM, Zimmer G. The fusion protein of respiratory syncytial virus triggers p53-dependent apoptosis. *J Virol* **2008**; 82: 3236–49. doi:10.1128/jvi.01887-07
8. Gower TL, Pastey MK, Peeples ME, Collins PL, McCurdy LH, Hart TK, *et al.* RhoA signaling is required for respiratory syncytial virus-induced syncytium formation and filamentous virion morphology. *J Virol* **2005**; 79: 5326–36. doi:10.1128/jvi.79.9.5326-5336.2005
9. Schlender J, Walliser G, Fricke J, Conzelmann KK. Respiratory syncytial virus fusion protein mediates inhibition of mitogen-induced T-cell proliferation by contact. *J Virol* **2002**; 76: 1163–70. doi:10.1128/jvi.76.3.1163-1170.2002
10. Griffiths CD, Bilawchuk LM, McDonough JE, Jamieson KC, Elawar F, Cen Y, *et al.* IGF1R is an entry receptor for respiratory syncytial virus. *Nature* **2020**; 583: 615–9. doi:10.1038/s41586-020-2369-7
11. Mastrangelo P, Chin AA, Tan S, Jeon AH, Ackerley CA, Siu KK, *et al.* Identification of RSV Fusion Protein Interaction Domains on the Virus Receptor, Nucleolin. *Viruses* **2021**; 13: 261. doi:10.3390/v13020261
12. Kojima R, Bojar D, Rizzi G, Hamri GC-E, El-Baba MD, Saxena P, et al. Designer exosomes produced by implanted cells intracerebrally deliver therapeutic cargo for Parkinson's disease treatment. *Nat Commun* **2018**; 9: 1305. doi:10.1038/s41467-018-03733-8
13. Rezabakhsh A, Sokullu E, Rahbarghazi R. Applications, challenges and prospects of mesenchymal stem cell exosomes in regenerative medicine. *Stem Cell Res Ther* **2021**; 12: 521. doi:10.1186/s13287-021-02596-z
14. Chan MH, Chang ZX, Huang CF, Lee LJ, Liu RS, Hsiao M. Integrated therapy platform of exosomal system: hybrid inorganic/organic nanoparticles with exosomes for cancer treatment. *Nanoscale Horiz* **2022**; 7: 352–67. doi:10.1039/d1nh00637a
15. Hade MD, Suire CN, Suo Z. Mesenchymal Stem Cell-Derived Exosomes: Applications in Regenerative Medicine. *Cells* **2021**; 10: 1959. doi:10.3390/cells10081959
16. Munagala R, Aqil F, Jeyabalan J, Kandimalla R, Wallen M, Tyagi N, *et al.* Exosome-mediated delivery of RNA and DNA for gene therapy. *Cancer Lett* **2021**; 505: 58–72. doi:10.1016/j.canlet.2021.02.011
17. Lan F, Qing Q, Pan Q, Hu M, Yu H, Yue X. Serum exosomal miR-301a as a potential diagnostic and prognostic biomarker for human glioma. *Cell Oncol (Dordr)* **2018**; 41: 25–33. doi:10.1007/s13402-017-0355-3
18. Hong S, Ruan S, Greenberg Z, He M, McGill JL. Development of surface engineered antigenic exosomes as vaccines for respiratory syncytial virus. *Sci Rep* **2021**; 11: 21358. doi:10.1038/s41598-021-00765-x
19. Zhang M, Hu S, Liu L, Dang P, Liu Y, Sun Z, *et al.* Engineered exosomes from different sources for cancer-targeted therapy. *Signal Transduct Target Ther* **2023**; 8: 124. doi:10.1038/s41392-023-01382-y
20. Corbeau A, Kuipers SC, de Boer SM, Horeweg N, Hoogeman MS, Godart J, *et al.* Correlations between bone marrow radiation dose and hematologic toxicity in locally advanced cervical cancer patients receiving chemoradiation with cisplatin: a systematic review. *Radiother Oncol* **2021**; 164: 128–37. doi:10.1016/j.radonc.2021.09.009
21. Ferrari P, Scatena C, Ghilli M, Bargagna I, Lorenzini G, Nicolini A. Molecular Mechanisms, Biomarkers and Emerging Therapies for Chemotherapy Resistant TNBC. *Int J Mol Sci* **2022**; 23: 1665. doi:10.3390/ijms23031665
22. Wikramanayake TC, Haberland NI, Akhundlu A, Laboy Nieves A, Miteva M. Prevention and Treatment of Chemotherapy-Induced Alopecia: What Is Available and What Is Coming? *Curr Oncol* **2023**; 30: 3609–26. doi:10.3390/curroncol30040275
23. Ruddy KJ, Patel SR, Higgins AS, Armenian SH, Herrmann J. Cardiovascular Health during and after Cancer Therapy. *Cancers (Basel)* **2020**; 12: 3737. doi:10.3390/cancers12123737
24. Was H, Borkowska A, Bagues A, Tu L, Liu JYH, Lu Z, *et al.* Mechanisms of Chemotherapy-Induced Neurotoxicity. *Front Pharmacol* **2022**; 13: 750507. doi:10.3389/fphar.2022.750507
25. Schofield J, Harcus M, Pizer B, Jorgensen A, McWilliam S. Long-term cisplatin nephrotoxicity after childhood cancer: a systematic review and meta-analysis. *Pediatr Nephrol* **2024**; 39: 699–710. doi:10.1007/s00467-023-06149-9
26. Taghipour YD, Zarebkohan A, Salehi R, Talebi M, Rahbarghazi R, Khordadmehr M, *et al.* Enhanced docetaxel therapeutic effect using dual targeted SRL-2 and TA1 aptamer conjugated micelles in inhibition Balb/c mice breast cancer model. *Sci Rep* **2024**; 14: 24603. doi:10.1038/s41598-024-75042-8
27. Chen Y, Feng X, Yuan Y, Jiang J, Zhang P, Zhang B. Identification of a novel mechanism for reversal of doxorubicin-induced chemotherapy resistance by TXNIP in triple-negative breast cancer via promoting reactive oxygen-mediated DNA damage. *Cell Death Dis* **2022**; 13: 338. doi:10.1038/s41419-022-04783-z
28. Swedan HK, Kassab AE, Gedawy EM, Elmeligie SE. Topoisomerase II inhibitors design: Early studies and new perspectives. *Bioorg Chem* **2023**; 136: 106548. doi:10.1016/j.bioorg.2023.106548
29. Mahmoud R, Ordóñez-Morán P, Allegrucci C. Challenges for Triple Negative Breast Cancer Treatment: Defeating Heterogeneity and Cancer Stemness. *Cancers (Basel)* **2022**; 14: 4280. doi:10.3390/cancers14174280
30. Wei L, Kim SH, Armaly AM, Aubé J, Xu L, Wu X. HuR inhibition overcomes cFLIP-mediated doxorubicin resistance in triple-negative breast cancer. *NPJ Precis Oncol* **2024**; 8: 286. doi:10.1038/s41698-024-00780-x
31. Li Y, Tang T, Sun Y, Chen G, Yuan X, Cai D. The role of TLR-4 in chemoresistance of cancer. *Discov Oncol* **2025**; 16: 865. doi:10.1007/s12672-025-02509-z
32. Fonseca NA, Rodrigues AS, Rodrigues-Santos P, Alves V, Gregório AC, Valério-Fernandes Â, *et al.* Nucleolin overexpression in breast cancer cell sub-populations with different stem-like phenotype enables targeted intracellular delivery of synergistic drug combination. *Biomaterials* **2015**; 69: 76–88. doi:10.1016/j.biomaterials.2015.08.007
33. Ma Y, Xie D, Chen Z, Shen X, Wu X, Ding F, *et al.* Advancing targeted combination chemotherapy in triple negative breast cancer: nucleolin aptamer-mediated controlled drug release. *J Transl Med* **2024**; 22: 604. doi:10.1186/s12967-024-05429-8
34. Kumar S, Chaudhri S. Recent update on IGF-1/IGF-1R signaling

axis as a promising therapeutic target for triple-negative breast cancer. *Pathol Res Pract* **2024**; 263: 155620. doi:10.1016/j.prp.2024.155620
35. Farabaugh SM, Boone DN, Lee AV. Role of IGF1R in Breast Cancer Subtypes, Stemness, and Lineage Differentiation. *Front Endocrinol (Lausanne)* **2015**; 6: 59. doi:10.3389/fendo.2015.00059
36. Ju H, Hu Z, Lu Y, Wu Y, Zhang L, Wei D, *et al.* TLR4 activation leads to anti-EGFR therapy resistance in head and neck squamous cell carcinoma. *Am J Cancer Res* **2020**; 10: 454–72.
37. Carvalho LS, Gonçalves N, Fonseca NA, Moreira JN. Cancer Stem Cells and Nucleolin as Drivers of Carcinogenesis. *Pharmaceuticals (Basel)* **2021**; 14: 60. doi:10.3390/ph14010060
38. De S, Zhou H, DeSantis D, Croniger CM, Li X, Stark GR. Erlotinib protects against LPS-induced endotoxicity because TLR4 needs EGFR to signal. *Proc Natl Acad Sci U S A* **2015**; 112: 9680-9685. doi:10.1073/pnas.1511794112
39. Mazloumi Z, Rafat A, Dizaji Asl K, Nozad Charoudeh H. A combination of telomerase inhibition and NK cell therapy increased breast cancer cell line apoptosis. *Biochem Biophys Res Commun* **2023**; 640: 50–5. doi:10.1016/j.bbrc.2022.11.090
40. Li M, Zhang Y, Wu B, Qiu R, Zhao C, Chen B, *et al.* Optimizing dose selection for doxorubicin-induced cardiotoxicity in mice: A comprehensive analysis of single and multiple-dose regimens. *Eur J Pharmacol* **2025**; 1003: 177883. doi:10.1016/j.ejphar.2025.177883
41. Stępień E, Kamińska A, Surman M, Karbowska D, Wróbel A, Przybyło M. Fourier-Transform InfraRed (FT-IR) spectroscopy to show alterations in molecular composition of EV subpopulations from melanoma cell lines in different malignancy. *Biochem Biophys Rep* **2021**; 25: 100888. doi:10.1016/j.bbrep.2020.100888
42. Soares Martins T, Magalhães S, Rosa IM, Vogelgsang J, Wiltfang J, Delgadillo I, *et al.* Potential of FTIR Spectroscopy Applied to Exosomes for Alzheimer's Disease Discrimination: A Pilot Study. *J Alzheimers Dis* **2020**; 74: 391–405. doi:10.3233/jad-191034
43. Zaheer J, Shanmugiah J, Kim S, Kim H, Kim JS. Tumor microenvironment modulation by SERPINE1 increases radioimmunotherapy in murine model of gastric cancer. *Sci Rep* **2025**; 15: 16449. doi:10.1038/s41598-025-97983-4
44. Su YH, Wu YZ, Ann DK, Chen JL, Kuo CY. Obesity promotes radioresistance through SERPINE1-mediated aggressiveness and DNA repair of triple-negative breast cancer. *Cell Death Dis* **2023**; 14: 53. doi:10.1038/s41419-023-05576-8
45. Mitchel JA, Das A, O'Sullivan MJ, Stancil IT, DeCamp SJ, Koehler S, *et al.* In primary airway epithelial cells, the unjamming transition is distinct from the epithelial-to-mesenchymal transition. *Nat Commun* **2020**; 11: 5053. doi:10.1038/s41467-020-18841-7
46. Chen L, Lin G, Chen K, Liang R, Wan F, Zhang C, *et al.* VEGF promotes migration and invasion by regulating EMT and MMPs in nasopharyngeal carcinoma. *J Cancer* **2020**; 11: 7291–301. doi:10.7150/jca.46429
47. Musick M, Ufondu CA, Rowland CE, Sottnik JL, Shackleford MT, Nesiba CS, *et al.* CDH1 loss remodels gene expression and lineage identity in human mammary epithelial cells. *bioRxiv* **2025**. doi:10.1101/2025.06.20.660633 Shenoy S. CDH1 (E-Cadherin) Mutation and Gastric Cancer: Genetics, Molecular Mechanisms and Guidelines for Management. *Cancer Manag Res* **2019**; 11: 10477–86. doi:10.2147/cmar.S208818
48. Reshmitha TR, Nisha P. Lycopene mitigates acrylamide and glycidamide induced cellular toxicity via oxidative stress modulation in HepG2 cells. *Journal of Functional Foods* **2021**; 80: 104390. doi:10.1016/j.jff.2021.104390
49. Soudi T, Bagheri F, Shojaosadati SA, Rezaei M, Motamedian E. Modified exosomes for targeted delivery of doxorubicin and carvedilol to mitochondria in breast cancer cells. *Sci Rep* 2025; 15: 38386. doi:10.1038/s41598-025-22156-2
50. Tian C, Yang Y, Bai B, Wang S, Liu M, Sun RC, *et al.* Potential of exosomes as diagnostic biomarkers and therapeutic carriers for doxorubicin-induced cardiotoxicity. *Int J Biol Sci* **2021**; 17: 1328–38. doi:10.7150/ijbs.58786
51. Liang Y, Duan L, Lu J, Xia J. Engineering exosomes for targeted drug delivery. *Theranostics* **2021**; 11: 3183–95. doi:10.7150/thno.52570
52. Jafari D, Shajari S, Jafari R, Mardi N, Gomari H, Ganji F, *et al.* Designer Exosomes: A New Platform for Biotechnology Therapeutics. *BioDrugs* **2020**; 34: 567–86. doi:10.1007/s40259-020-00434-x
53. Ramezani R, Mohammadian M, Hosseini ES, Zare M. The effect of bovine milk lactoferrin-loaded exosomes (exoLF) on human MDA-MB-231 breast cancer cell line. *BMC Complement Med Ther* **2023**; 23: 228. doi:10.1186/s12906-023-04045-1
54. Moradi A, Shirangi A, Asadi M, Farokhi M, Gholami M, Aminianfar H, *et al.* Targeted delivery of doxorubicin by SP5-52 peptide conjugated exosome nanoparticles into lung tumor: An in vitro and in vivo study. *Journal of Drug Delivery Science and Technology* **2024**; 92: 105313. doi:10.1016/j.jddst.2023.105313
55. Song Y, Zhang H, Wang X, Geng X, Sun Y, Liu J, *et al.* One Stone, Three Birds: pH Triggered Transformation of Aminopyronine and Iminopyronine Based Lysosome Targeting Viscosity Probe for Cancer Visualization. *Anal Chem* **2021**; 93: 1786–91. doi:10.1021/acs.analchem.0c04644
56. Farshbaf M, Mojarad-Jabali S, Hemmati S, Khosroushahi AY, Motasadizadeh H, Zarebkohan A, *et al.* Enhanced BBB and BBTB penetration and improved anti-glioma behavior of Bortezomib through dual-targeting nanostructured lipid carriers. *J Control Release* **2022**; 345: 371–84. doi:10.1016/j.jconrel.2022.03.019
57. Qi L, Ge W, Pan C, Jiang W, Lin D, Zhang L. Compromised osteogenic effect of exosomes internalized by senescent bone marrow stem cells via endocytoses involving clathrin, macropinocytosis and caveolae. *Front Bioeng Biotechnol* **2022**; 10: 1090914. doi:10.3389/fbioe.2022.1090914
58. Xu L, Faruqu FN, Liam-Or R, Abu Abed O, Li D, Venner K, *et al.* Design of experiment (DoE)-driven in vitro and in vivo uptake studies of exosomes for pancreatic cancer delivery enabled by copper-free click chemistry-based labelling. *J Extracell Vesicles* **2020**; 9: 1779458. doi:10.1080/20013078.2020.1779458
59. Li H, Xu W, Li F, Zeng R, Zhang X, Wang X, *et al.* Amplification of anticancer efficacy by co-delivery of doxorubicin and lonidamine with extracellular vesicles. *Drug Deliv* **2022**; 29: 192–202. doi:10.1080/10717544.2021.2023697
60. Karahmet Sher E, Alebić M, Marković Boras M, Boškailo E, Karahmet Farhat E, Karahmet A, *et al.* Nanotechnology in medicine revolutionizing drug delivery for cancer and viral infection treatments. *Int J Pharm* **2024**; 660: 124345. doi:10.1016/j.ijpharm.2024.124345
61. Attaianese F, Guiducci S, Trapani S, Barbati F, Lodi L, Indolfi G, *et al.* Reshaping Our Knowledge: Advancements in Understanding the Immune Response to Human Respiratory Syncytial Virus. *Pathogens* **2023**; 12: 1118. doi:10.3390/pathogens12091118
62. Tang J, Zhou B, Scott MJ, Chen L, Lai D, Fan EK, *et al.* EGFR signaling augments TLR4 cell surface expression and function in macrophages via regulation of Rab5a activation. *Protein Cell* **2020**; 11: 144–9. doi:10.1007/s13238-019-00668-8
63. Liu J, Zhu C, Xu L, Wang D, Liu W, Zhang K, *et al.* Nanoenabled Intracellular Calcium Bursting for Safe and Efficient Reversal of Drug Resistance in Tumor Cells. *Nano Lett* **2020**; 20: 8102–11. doi:10.1021/acs.nanolett.0c03042
64. Persi E, Duran-Frigola M, Damaghi M, Roush WR, Aloy P, Cleveland JL, *et al.* Systems analysis of intracellular pH vulnerabilities for cancer therapy. *Nat Commun* **2018**; 9: 2997. doi:10.1038/s41467-018-05261-x
65. Cheng X, Xu HD, Ran HH, Liang G, Wu FG. Glutathione-Depleting Nanomedicines for Synergistic Cancer Therapy. *ACS Nano* **2021**; 15: 8039–68. doi:10.1021/acsnano.1c00498
66. Halim VA, García-Santisteban I, Warmerdam DO, van den Broek B, Heck AJR, Mohammed S, *et al.* Doxorubicin-induced DNA Damage Causes Extensive Ubiquitination of Ribosomal Proteins Associated with a Decrease in Protein Translation. *Mol Cell Proteomics* **2018**; 17: 2297–308. doi:10.1074/mcp.RA118.000652
67. Kozak J, Forma A, Czeczelewski M, Kozyra P, Sitarz R, Radzikowska-Büchner E, *et al.* Inhibition or Reversal of the Epithelial-Mesenchymal Transition in Gastric Cancer: Pharmacological Approaches. *Int J Mol Sci* **2020**; 22: 277. doi:10.3390/ijms22010277
68. Mathew C, Tamir S, Tripp RA, Ghildyal R. Reversible disruption of XPO1-mediated nuclear export inhibits respiratory syncytial virus (RSV) replication. *Sci Rep* **2021**; 11: 19223. doi:10.1038/s41598-021-98767-2

69. Salinas-Jazmín N, Medina-Mondragón MA, Jiménez-López J, Guerrero-Rodríguez SL, Cuautle-Rodríguez P, Velasco-Velázquez MA. Continuous exposure to doxorubicin induces stem cell-like characteristics and plasticity in MDA-MB-231 breast cancer cells identified with the SORE6 reporter. *Cancer Chemother Pharmacol* **2024**; 94: 571–83. doi:10.1007/s00280-024-04701-4
70. Xu B, Bai Z, Yin J, Zhang Z. Global transcriptomic analysis identifies SERPINE1 as a prognostic biomarker associated with epithelial-to-mesenchymal transition in gastric cancer. *PeerJ* **2019**; 7: e7091. doi:10.7717/peerj.7091
71. Nowicki A, Kulus M, Wieczorkiewicz M, Pieńkowski W, Stefańska K, Skupin-Mrugalska P, *et al.* Ovarian Cancer and Cancer Stem Cells-Cellular and Molecular Characteristics, Signaling Pathways, and Usefulness as a Diagnostic Tool in Medicine and Oncology. *Cancers (Basel)* **2021**; 13: 4178. doi:10.3390/cancers13164178
72. Paramanantham A, Jung EJ, Kim HJ, Jeong BK, Jung JM, Kim GS, *et al.* Doxorubicin-Resistant TNBC Cells Exhibit Rapid Growth with Cancer Stem Cell-like Properties and EMT Phenotype, Which Can Be Transferred to Parental Cells through Autocrine Signaling. *Int J Mol Sci* **2021**; 22: 12438. doi:10.3390/ijms222212438
73. Lambert AW, Weinberg RA. Linking EMT programmes to normal and neoplastic epithelial stem cells. *Nat Rev Cancer* **2021**; 21: 325–38. doi:10.1038/s41568-021-00332-6
74. Phi LTH, Sari IN, Yang YG, Lee SH, Jun N, Kim KS, *et al.* Cancer Stem Cells (CSCs) in Drug Resistance and their Therapeutic Implications in Cancer Treatment. *Stem Cells Int* **2018**; 2018: 5416923. doi:10.1155/2018/5416923
75. Li Y, He J, Wang F, Wang X, Yang F, Zhao C, *et al.* Role of MMP-9 in epithelial-mesenchymal transition of thyroid cancer. *World J Surg Oncol* **2020**; 18: 181. doi:10.1186/s12957-020-01958-w
76. Chen HH, Zhou XL, Shi YL, Yang J. Roles of p38 MAPK and JNK in TGF-β1-induced human alveolar epithelial to mesenchymal transition. *Arch Med Res* **2013**; 44: 93–8. doi:10.1016/j.arcmed.2013.01.004
77. Zhang J, Tian XJ, Zhang H, Teng Y, Li R, Bai F, *et al.* TGF-β-induced epithelial-to-mesenchymal transition proceeds through stepwise activation of multiple feedback loops. *Sci Signal* **2014**; 7: ra91. doi:10.1126/scisignal.2005304
78. Ashkar F, Wu J. E-Cadherin and its signaling pathways: A novel target of dietary components in modulating cell migration and proliferation. *Trends in Food Science & Technology* **2024**; 146: 104398. doi:https://doi.org/10.1016/j.tifs.2024.104398
79. Cui X, Shan T, Qiao L. Collagen type IV alpha 1 (COL4A1) silence hampers the invasion, migration and epithelial-mesenchymal transition (EMT) of gastric cancer cells through blocking Hedgehog signaling pathway. *Bioengineered* **2022**; 13: 8972–81. doi:10.1080/21655979.2022.2053799
80. Mailloux RJ. An Update on Mitochondrial Reactive Oxygen Species Production. *Antioxidants (Basel)* **2020**; 9: 472. doi:10.3390/antiox9060472
81. Byrd AS, O'Brien XM, Johnson CM, Lavigne LM, Reichner JS. An extracellular matrix-based mechanism of rapid neutrophil extracellular trap formation in response to Candida albicans. *J Immunol* **2013**; 190: 4136–48. doi:10.4049/jimmunol.1202671
82. Yang X, Liu X, Nie Y, Zhan F, Zhu B. Oxidative stress and ROS-mediated cellular events in RSV infection: potential protective roles of antioxidants. *Virol J* **2023**; 20: 224. doi:10.1186/s12985-023-02194-w
83. Surolia R, Antony VB. Pathophysiological Role of Vimentin Intermediate Filaments in Lung Diseases. *Front Cell Dev Biol* **2022**; 10: 872759. doi:10.3389/fcell.2022.872759